Fibre Optic Sensor Based on the Linear and Nonlinear Interaction

By

Kuja, Stanley Okoth

A thesis submitted to the School of Science, University of Eldoret, in partial fulfillment of the requirement for the degree of Master of Science in Physics.

MARCH 2013

DECLARATION

DECLARATION BY THE STUDENT

This thesis is my own original work presented to University of Eldoret. The work has not been presented for award of any degree in any other university. No part of this research work may be reproduced without prior knowledge of the author and University of Eldoret.

Kuja, Stanley Okoth,

SC/PGP/017/09,

Signature……. Date……

DECLARATION BY THE SUPERVISORS

This thesis has been submitted for examination with our approval as university supervisors

Dr. David W. Waswa,
Department of Physics,
University of Eldoret,
P.o. Box 1125,
Eldoret.

Signature……. Date……

Prof. George Amolo,
Department of Physics,
University of Eldoret,
P.o. Box 1125,
Eldoret.

Signature……. Date……

DEDICATION

To our Lord God who gives wisdom: out of our mouths comes knowledge and understanding.

ABSTRACT

In recent years the implementation of Erbium-doped fibre amplifiers has allowed the extension of high-bit rate transmission over long-haul distances. But the demand for an increase in transmission capacity is unprecedented and grows continuously. Despite the intrinsically small values of the nonlinear coefficient for silica, the nonlinear birefringence effects in optical fibres can be observed even at low powers considering that the light is confined in a relatively small area over long (i.e. transoceanic) interaction lengths due to the extremely low attenuation coefficient and the event of optical amplifiers. Due to this, nonlinear birefringence effects cannot be ignored when considering light propagation in optical fibres. In this research, both theoretical and experimental investigation of the interaction between linear and nonlinear induced birefringence in a fibre and the possibility of using this interaction to design fibre optic sensors (FOS) was done. Investigations show that the linear birefringence effect leads to a distortion of the signal but when it is frequency independent, its overall effect is just a rotation of the signal state of polarization (SOP) on the Poincaré sphere. Further investigation show that the effect of nonlinear birefringence alone depolarizes the signal, while in high polarization mode dispersion (PMD) links where polarization mode coupling is high, the linear and nonlinear birefringence vectors couple together such that it may reduce the penalty and improve the signal degree of polarization (DOP). As the channel spacing increases, the interaction between the probe and the pump signal is reduced, thus the DOP improvement for 100 GHz (0.8 nm) come later, after that of 50 GHz (0.4 nm) channel spacing. In optical sensing, the study show that the DOP of the probe increases linearly with the applied physical measurand (stress, strain, temperature). Also, the study shows that for temperature sensing with polarization maintaining fibre (PMF) used as a sensing fibre, the rate or frequency at which the DOP varies is faster at high temperatures than at lower temperatures. The design of a stress sensor gave the best sensitivity of 0.051 kg^{-1} over a range of 0-27.5 kg with PMF as the sensing fibre and 0.049 kg^{-1} over a range of 0-15 kg with LEAF as the sensing fibre. In strain sensing, a sensitivity of 0.0103 μm^{-1} was obtained with single mode fibre (SMF) as the sensing element. Lastly, the design of a temperature sensor gave the best sensitivity of 0.181 $^0C^{-1}$ with PMF fibre and 0.0009 $^0C^{-1}$ with SMF, thus, PMF fibre would be the best choice as a sensing element. The designed sensors offer a unique possibility in high accuracy and sensitivity at low powers than other polarimetric sensors.

TABLE OF CONTENTS

LIST OF FIGURES

LIST OF ABBREVIATIONS AND SYMBOLS

C-NLSE – Coupled Nonlinear Schrodinger Equation

CW – Continuous Wave

DGD – Differential Group Delay

DOP - Degree of Polarization

DSF – Dispersion Shifted Fibre

EDFA- Erbium-doped Fibre Optic Amplifier

FFT - Fast Fourier Transform

FOPMD – First Order Polarization Mode Dispersion

FOS – Fibre Optic Sensor

FWM- Four Wave Mixing

GVD - Group Velocity Dispersion

ICT - Information Communication Technology

LEAF – Large Effective Area Fibre

NPR – Nonlinear Polarization Rotations

OFDM - Orthogonal Frequency-Division Multiplexing

PC - Polarization Controller

PCD – Polarization Dependent Chromatic Dispersion

PDL – Polarization Dependent Loss

PFOS – Polarization-based Fibre Optic Sensor

PMD – Polarization Mode Dispersion

PMF – Polarization Maintaining Fibre

PSP - Principal State of Polarization

SMF - Single Mode Fibre

SOP - State of Polarization

SOPMD – Second Order Polarization Mode Dispersion

SPM - Self Phase Modulation

SSFM - Split Step Fourier Method

WDM - Wavelength Division Multiplexing

XPM - Cross Phase Modulation

LIST OF SYMBOLS

ω – Angular frequency

α – Attenuation constant

$\Delta\beta$ – Modal birefringence

γ – Nonlinear coefficient

Vg– Group velocity

θ – Relative angle between the pump and the probe

λ – Wavelength

$\Delta\tau$ – Differential group delay

L_B – Beat length

A_{eff} – Effective area

χ – Susceptibility of the medium

Ω – PMD vector

k – Propagation constant

c – Speed of light

Δn – Differential refractive index between the slow and fast modes

ACKNOWLEDGEMENT

I would like to begin by thanking my supervisors Dr. David W. Waswa and Prof. George Amolo for their support, criticism, pieces of advice throughout my Masters program and the persistent pushes to have me finish. In particular, I would like to thank Dr. Waswa for the frequent constructive discussions, his unique and attractive ways of assistance in understanding the field and of course, for the research travel to S. Africa. Sincere gratitude also goes to Physics Department for giving me an opportunity to undertake my project work using departmental resources.

I am greatly indebted to my late parents, Mr & Mrs Kuja for planting the virtue of hard work and patience, my brothers Humphrey and Maviri Diang'a, my lovely sisters Zamedi and Nyamakoma, and the entire Nyakado family, whose unbound love, moral, material and financial support and encouragement has helped me during the time of my research and studies at the university.

I wish to thank Dr. Makau for providing inspiration to work hard and his constant pieces of advice across the board: a level minded person indeed. I remain indebted to my fellow research group members (Rotich and Boiyo), Moro, Easter, Iris, Mathews and Atambo for their truly invaluable collaboration, encouragement and advice.

I gratefully acknowledge the three month South Africa visit funding by African Laser Centre (ALC) and Prof. Andrew Leitch of Nelson Mandela Metropolitan University (NMMU). Sincere thanks also goes to Fibre Optic Research Lab; Dr. Tim Gibbon (South Africa), Romeo G. (Namibia), K Muguro (Kenya) and NMMU generally, for their support and contribution. To each of the above I extend my deepest appreciation and their extreme generosity will be remembered always. Glory be to God, who makes all things possible.

CHAPTER 1

INTRODUCTION

1.1 Background

From ancient times till now, civilizations have advanced as people discovered new ways of exploiting various physical resources such as materials, fundamental forces and energies. In the recent past, information technology was added to the list when computers allowed complex information processing to be performed outside human brains. There is now a move towards a society which requires that one accesses information at their finger tips when they need it, where they need it, and in whatever format they need it. Fibre-optic technology can be considered to be the solution for meeting the above need because of its potentially limitless capabilities, huge bandwidth (in terms of Tb/s), low signal attenuation (0.2 dB/km), low signal distortion, low power requirement, low material usage, small space requirement and low cost [1, 2]. The exponential rise in the demand for high speed optical communication systems [3] has forced networks to use higher bit rates and transmission powers.

Optical fibres have become an important transmission medium but, of course, such transmission is never perfect and non-ideal behaviour leads to limitations in the performance of communication systems, based on optical fibres. The two polarization states in an ideal, perfectly circular optical fibre are degenerate, so the propagation wave number does not depend on the polarization state. Real optical fibres are never perfect, they have slight asymmetries or other perturbations that destroy the degeneracy, leading to two polarization states with slightly different phase and group velocities, a

phenomenon known as birefringence [4]. The birefringence in the fibre contributes to polarization mode dispersion (PMD) which is a major limiting factor that leads to system impairments for the transmission of high speed optical signals over the already embedded optical fibre network. Digital signal propagating through an optical fibre with linear birefringence effects may be broadened during transmission and as a consequence spread beyond their allocated bit slot and interfere with neighbouring bits. The distortion introduced by linear birefringence becomes relevant for systems operating at bit rate larger than 10 Gb/s per channel. The introduction of optical amplifiers has allowed a considerable increase in the length of the communication link, which in turn has also allowed linear effects to accumulate over even longer distances.

Nonlinear effects become significant at high optical power levels and have become more important since the development of Erbium-doped fibre amplifier (EDFA) and wavelength division multiplexed (WDM) systems. By increasing the capacity of the optical transmission line, which can be achieved by increasing channel bit rate, decreasing channel spacing or the combination of both, the fibre nonlinearities come to play an even more decisive role on the signal transmission.

The origin of the nonlinearities is the refractive index of the optical fibre, which varies with the intensity of the optical signal. The high signal intensity associated with the large number of channels at closely spaced wavelengths may introduce problematic nonlinear effects; such as four-wave mixing (FWM), self-phase modulation (SPM) and cross-phase modulation (XPM). Thus, the intensity dependence of the refractive index

(optical Kerr effect) is responsible for nonlinear birefringence whose effect is nonlinear polarization rotation [5]. These effects just like the linear effects can be detrimental in optical communications, but they also, have many useful applications, especially for the implementation of all-optical functionalities in optical networks [6]. It is therefore, important to analyze the interaction between the linear and nonlinear effects in the transmission system in order to utilize their potential to the fullest.

The analysis of the interaction between the linear and nonlinear birefringence may lead to design of various optical devices such as optical switches and sensors. Fibre optic sensors have been employed in a variety of applications, including in composite materials, remote sensing, and monitoring of hazardous environment since they have several advantages such as small size and weight, immunity to electromagnetic interferences, intrinsically safe in explosive environments and high multiplexing potentials. A number of intrinsic and extrinsic fibre sensors have been developed in the past few years. Intrinsic fibre sensors fall into the category of polarimetric sensors through the employment of high birefringent polarization maintaining fibres as sensing elements. In spite of many advantages, there is growing demand for improved sensitivity, reliability, accuracy, flexibility and better compatibility of fibre optic sensors for various applications.

1.2 Problem Statement

Signal impairment effects due to optical birefringence introduced through intrinsic or extrinsic perturbations seriously degrade network performance. Thus, there is need to

investigate effects of linear and nonlinear optical birefringence in order that they be fully understood and also, ensure that they contribute constructively to the transfer of information in a fibre and in designing of optical devices such as optical switches and sensors. Efficient data monitoring in fibre transmission links through network sensing require very sensitive and easier to install sensors, making fibre optic sensors to be the perfect choice. Also, monitoring environmental changes such as temperature variations and impending landslides remains a key challenge, since it requires very reliable and accurate sensors; this paves the way for optical sensing.

1.3 Objectives

i. To investigate the effect of linear and nonlinear birefringence on the signal transmission.

ii. To study the possibility of using the nonlinear polarization coupling to develop an optical sensor.

1.4 Significance

The demand for an increase in transmission capacity is unprecedented and grows continuously e.g. in broadband access to the Internet. A sound knowledge on the useful exploitation of the interaction between the linear and nonlinear induced birefringence to the design of fibre optic sensors is necessary. Also, it will be a major contribution in the communication industry as far as Information and Communication Technology (ICT) is concerned, for example biometric voter registration. Optical sensing would have a variety of applications, for example, in biomedical applications where the interesting

temperature range is relatively narrow, in agriculture to monitor temperature inside the green houses, in fuselage or buildings for monitoring the structure's strain and temperature, among others.

CHAPTER 2

LITERATURE REVIEW

2.1 Linear Effects in Optical Fibres

An optical fibre is a cylindrical thin hair like dielectric material (glass or plastic) that acts like an optical wire. When a dielectric material is subjected to an electric field, a slight displacement will occur between the electrons and the ion cores. These small movements (ion cores in one direction and electrons in the opposite direction) will result in an induced electric dipole moment that leads to polarization, a phenomenon which plays an important role in the interaction of light with matter.

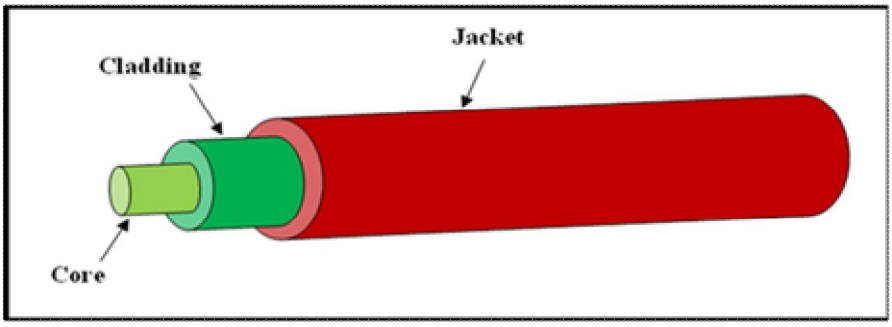

Fig. 2.1: Diagram showing a section of fibre.

2.1.1 Concept of Polarized Light

Polarization is a property of electromagnetic radiation describing the shape and the orientation of the electric field vector as a function of time, at a given point in space. If light is assumed to propagate in the positive z-direction, the real instantaneous electric field vectors along x-axis and y-axis can be written as

$$\vec{E}_x(z,t) = E_{0x}\cos(kz-\omega t)\vec{x} \quad , \quad \vec{E}_y(z,t) = E_{0y}\cos(kz-\omega t+\varepsilon)\vec{y} \ \ldots\ldots\ldots\ldots\ldots\ldots \quad (2.1)$$

where E_{0x} and E_{0y} are the maximum amplitudes in the x and y-axis, k is the propagation constant, ω is angular frequency, ε is the phase difference between the electric field vectors, and t is time. From Eq. (2.1), one can get the equation of an ellipse:

$$\left(\frac{E_x}{E_{0x}}\right)^2 + \left(\frac{E_y}{E_{0y}}\right)^2 - 2\frac{E_x}{E_{0x}}\frac{E_y}{E_{0y}}\cos\varepsilon = \sin^2\varepsilon \quad \text{..... (2.2)}$$

The trace of the state of polarization (SOP) is as shown in Fig. 2.2 and the angle α is the SOP orientation angle relative to the x-axis.

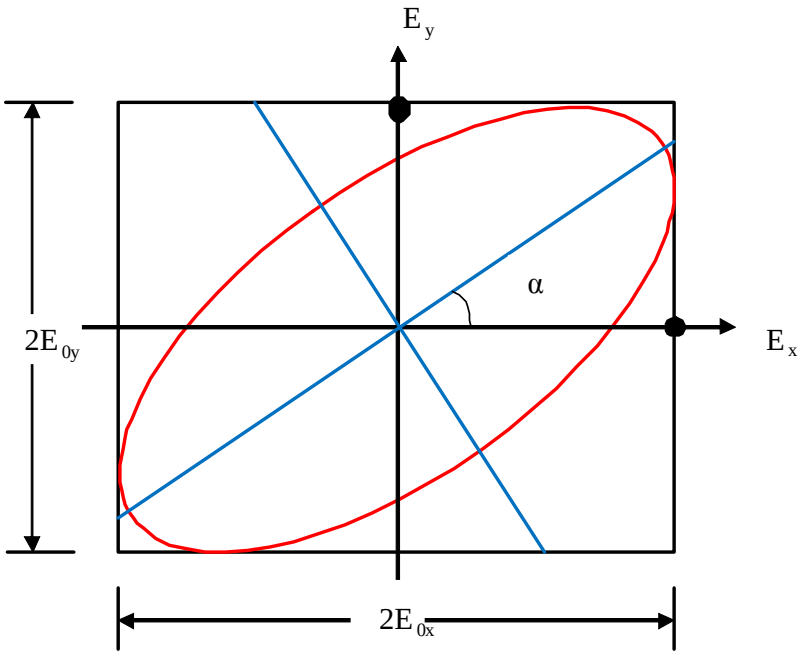

Fig. 2.2: Elliptically polarized light oriented at an angle relative to the x-axis having components of amplitude $2E_{0y}$ and $2E_{0x}$.

When the phase ε = ±nπ, (n = 0, 1, 2 …), the ellipse collapses into a straight line and it corresponds to a linearly polarized light with a constant orientation and varying amplitude. When ε = ±(2n+1) π/2, (n = 0, 1, 2 …), there is constant amplitude (E_{0x} = E_{0y}) but varying orientation giving circularly polarized light. Elliptically polarized light has both varying orientation and amplitude.

2.1.2 Jones and Stokes Formalism

The state of polarization of a signal at any given frequency can be uniquely represented by two parameters called Jones and Stokes vectors. A Jones vector is essentially a 2 by 1 unitary vector with complex components. Each complex component accounts for the magnitude and absolute phase of the electric field polarized in either the horizontal or vertical directions. The following equation represents the Jones vector [7]:

$$E = \begin{pmatrix} E_x \\ E_y \end{pmatrix} = \begin{pmatrix} E_{0x} e^{i\varphi_x} \\ E_{0y} e^{i\varphi_y} \end{pmatrix} \quad \text{..... (2.3)}$$

where φ_x and φ_y are phases of light wave in the x and y-axis. The use of Jones vectors to represent states of polarization provides a simple way of mathematically manipulating signals with a particular state of polarization. However, it becomes difficult to directly appreciate the changes in the state of polarization of a signal when the complex elements of a Jones vector change. In other words, Jones formalism can only deal with 100% polarization. However, in the general case, the propagating wave may consist of a polarized component and unpolarized component. Therefore, we resort to Stokes vector $\boldsymbol{S} = [S_0, S_1, S_2, S_3]$, which offer a qualitative way of representing a state of polarization of a propagating light-wave. The four Stokes parameters are given as:

$$\begin{aligned} S_0 &= E_{0x}^2 + E_{0y}^2 \\ S_1 &= E_{0x}^2 - E_{0y}^2 \\ S_2 &= 2E_{0x}E_{0y}\cos\ \varepsilon \\ S_3 &= 2E_{0x}E_{0y}\sin\ \varepsilon \end{aligned} \quad \text{..... (2.4)}$$

The three normalized Stokes vectors s_1, s_2, and s_3 are coordinates on the Poincaré sphere that define the unique state of polarization; with S_1 referring to vertical/horizontal polarizations, S_2 to the $+45^o$ or -45^o and S_3 to right/left circular polarization.

Linear polarizations are located on the equator, circular states are located at the poles with intermediate elliptical states continuously distributed between the equator and the poles as shown in Fig. 2.3. Right-hand and left-hand elliptical states occupy the northern and southern hemispheres, respectively. Because a state of polarization is represented by a point, a continuous evolution of state of polarization can be represented as a continuous path on the Poincaré sphere.

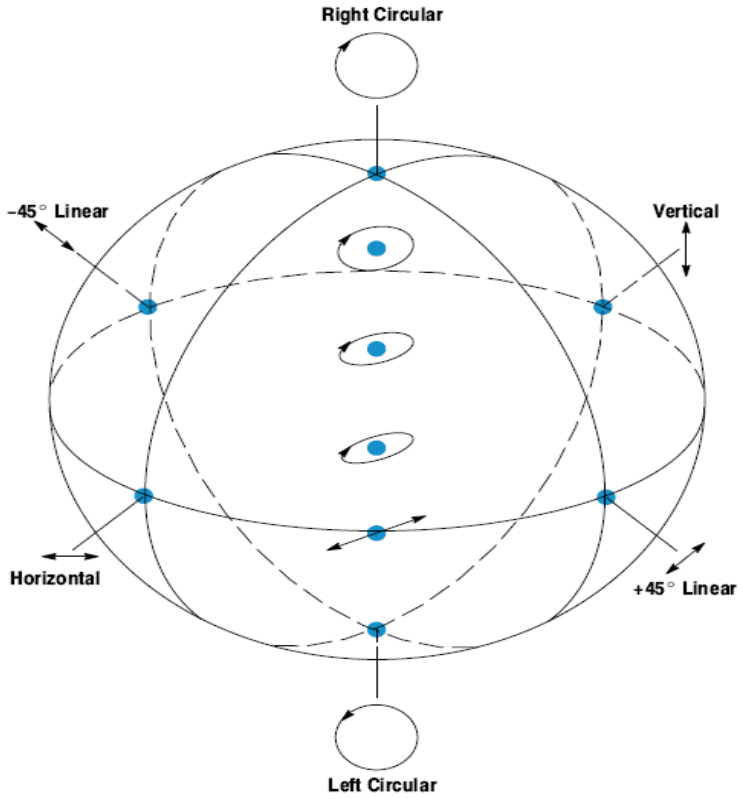

Fig. 2.3: Representation of different states of polarization on the Poincaré sphere.

The ratio of intensity of the polarized light to the total intensity gives a fundamental parameter in fibre optics known as degree of polarization (DOP) [8], given as:

$$DOP = \frac{I_{pol}}{I_{tol}} = \frac{\sqrt{S_1^{\,2} + S_2^{\,2} + S_3^{\,2}}}{S_0}, \quad 0 \le DOP \le 1 \ldots\ldots\ldots\ldots\ldots\ldots\ldots \quad (2.5)$$

where I_{tot} is the total intensity (polarized and unpolarized light), $I_{tot} = S_0$. If DOP = 0, the light signal is not polarized and its Stokes vector will be found within the volume of the Poincaré sphere while if DOP = 1, the light signal is completely polarized and the Stokes vector will be located on the surface of the unit sphere.

2.1.3 Polarization Mode Dispersion

Single-mode optical fibres ideally are supposed to maintain a single polarization state even after long distance transmission. In practice, the optical pulse propagates along single-mode fibre in two polarization modes due to asymmetry in the fibre cross-section [9]. The consequence of this asymmetry of cross-section is the existence of optical birefringence. As a result of birefringence, a pulse launched into the fibre at a particular state of polarization, split into two identical, linearly polarized pulses, having their electric field vectors aligned with the symmetry axes of the fibre and having different group velocities. The pulses arrive at the output differentially delayed as shown in Fig. 2.4. The difference in the transmission time of two pulses polarized along the states of polarization producing the shortest and longest propagation times is known as the *Differential Group Delay (DGD)* given by Eq. (2.6). The DGD is a measure of an effect known as polarization mode dispersion (PMD), which is a phenomenon that leads to pulse broadening and system impairments limiting the transmission capacity of the fibre [10, 11].

$$\Delta\tau = \left| \frac{L}{V_{gx}} - \frac{L}{V_{gy}} \right| = L\left|\beta_{1x} - \beta_{1y}\right| = L\left(\Delta\beta_1\right) \text{.....} \quad (2.6)$$

where $\Delta\tau$ is the differential group delay, L is the length of the fibre, V_{gx} and V_{gy} are the group velocities along the x and y directions and $\Delta\beta_1$ is the modal birefringence given by the difference in birefringence parameters $\Delta\beta_{1x}$ and $\Delta\beta_{1y}$.

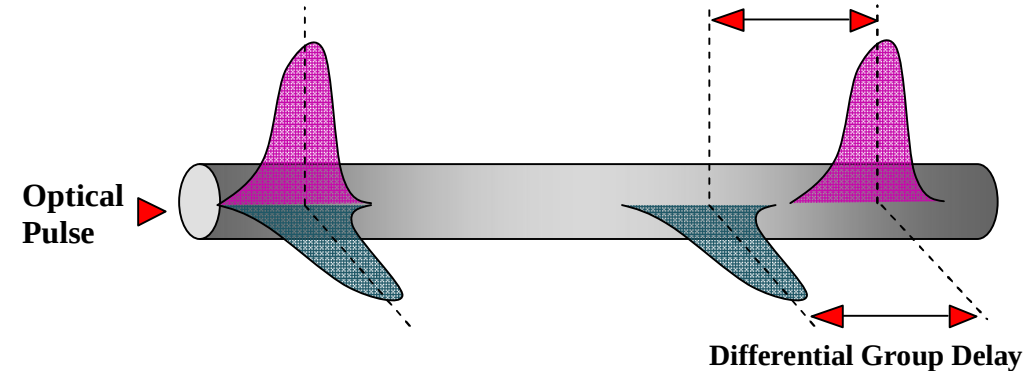

Fig. 2.4: Effect of PMD in a birefringent fibre on optical pulse.

2.1.4 Causes of Birefringence and Mode Coupling

As it has been mentioned earlier, PMD has its origin in optical birefringence and the causes of this birefringence are the intrinsic and extrinsic perturbations in optical fibre. Intrinsic perturbations include the manufacturing process such as drawing or cooling stage of fabrication which causes permanent birefringence, while extrinsic perturbations include stress which causes non circularity of the fibre core and environmental changes like temperature and pressure. These factors are illustrated in Fig. 2.5. The perturbations change as the fibre's external environment changes [12, 13].

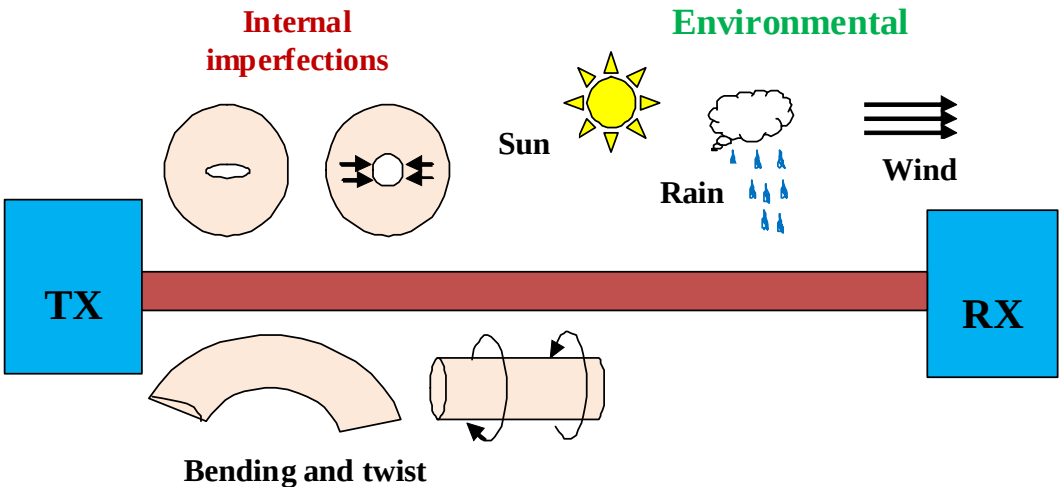

Fig. 2.5: Factors responsible for birefringence in optical fibre.

The birefringence difference between the fast and slow modes can be expressed as [14]:

$$\Delta\beta = \frac{\omega n_s}{c} - \frac{\omega n_f}{c} = \frac{\omega \Delta n}{c} \quad \text{..... (2.7)}$$

where ω is the angular optical frequency, c is the speed of light and $\Delta n = n_s - n_f$ is the differential refractive index between the slow and fast modes. Since each mode propagating through the fibre experiences different mode indexes, a phase lag is introduced between those two components at each frequency. This progressive slippage of the two orthogonally polarized modes will, in turn, cause the overall state of polarization of the signal to evolve with distance (refer to Fig. 2.6), effectively tracing out a circle on the surface of the Poincaré sphere.

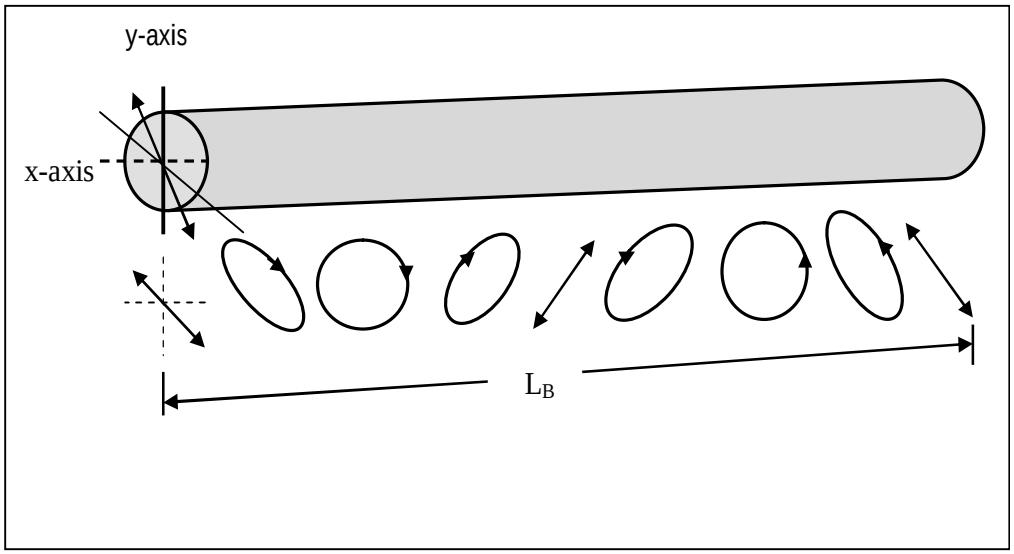

Fig. 2.6: Schematic illustration of polarization evolution and beat length L_B [15].

The distance over which the state of polarization undergoes a full rotation on the Poincaré sphere (i.e. experiences a phase shift of 2π between its components) is called the beat length and is given by:

$$L_B = \frac{\lambda}{\Delta n} = \frac{2\pi}{\Delta \beta} \quad \text{..... (2.8)}$$

2.1.5 Polarization Mode Coupling

In long fibres with various kinds of extrinsic and intrinsic perturbations as mentioned in subsection 2.1.4, there are random variations in the axes of the birefringence along the fibre length, causing random coupling of the two modes, known as polarization mode coupling. Mode coupling can also develop in long transmission systems, where the fibre link is composed of a large number of segments of single mode fibres having random lengths and random fusion angles between them. Each of these segments has its own

slow and fast modes and a portion of the signal propagates on each of them. At the boundary between the sections, the polarization vectors will be resolved into new pairs of local modes belonging to the next segment. The process of rotating the polarization vector into the new modes of the following segment is also known as mode coupling. Mode coupling becomes an issue for lengths longer than 100 m [16]. In general, PMD is caused by the birefringence in the fibre and is complicated by mode coupling in the fibre link.

The mode coupling process allows the DGD to increase proportionally to the square root of the length of the fibre link [17]. Similarly, the *polarization mode dispersion coefficient* is defined as the PMD divided by the square root of fibre length (measured in ps/$\sqrt{\text{km}}$). The DGD does not increase linearly with highly mode-coupled fibres because occasionally, the coupling between segments reduces the accumulated DGD i.e. when the slow mode of one segment is aligned with the fast mode of the next or previous segment, the DGD of both segments will cancel out. It is the mode coupling phenomenon which makes the DGD and the fast and slow modes of the fibre to be frequency dependent [18].

2.1.6 Linear Birefringence

In the absence of polarization dependent losses, the input (output) states of polarization are mutually orthogonal because there is nothing to break the degeneracy in the two supported modes. These states of polarization are commonly [19] referred to as *Principal States of Polarization (PSPs)*. The differential transmission time of two undistorted

signals polarized along mutually orthogonal states of polarization constitutes what it is known as the *linear birefringence effect* as shown in Fig. 2.7.

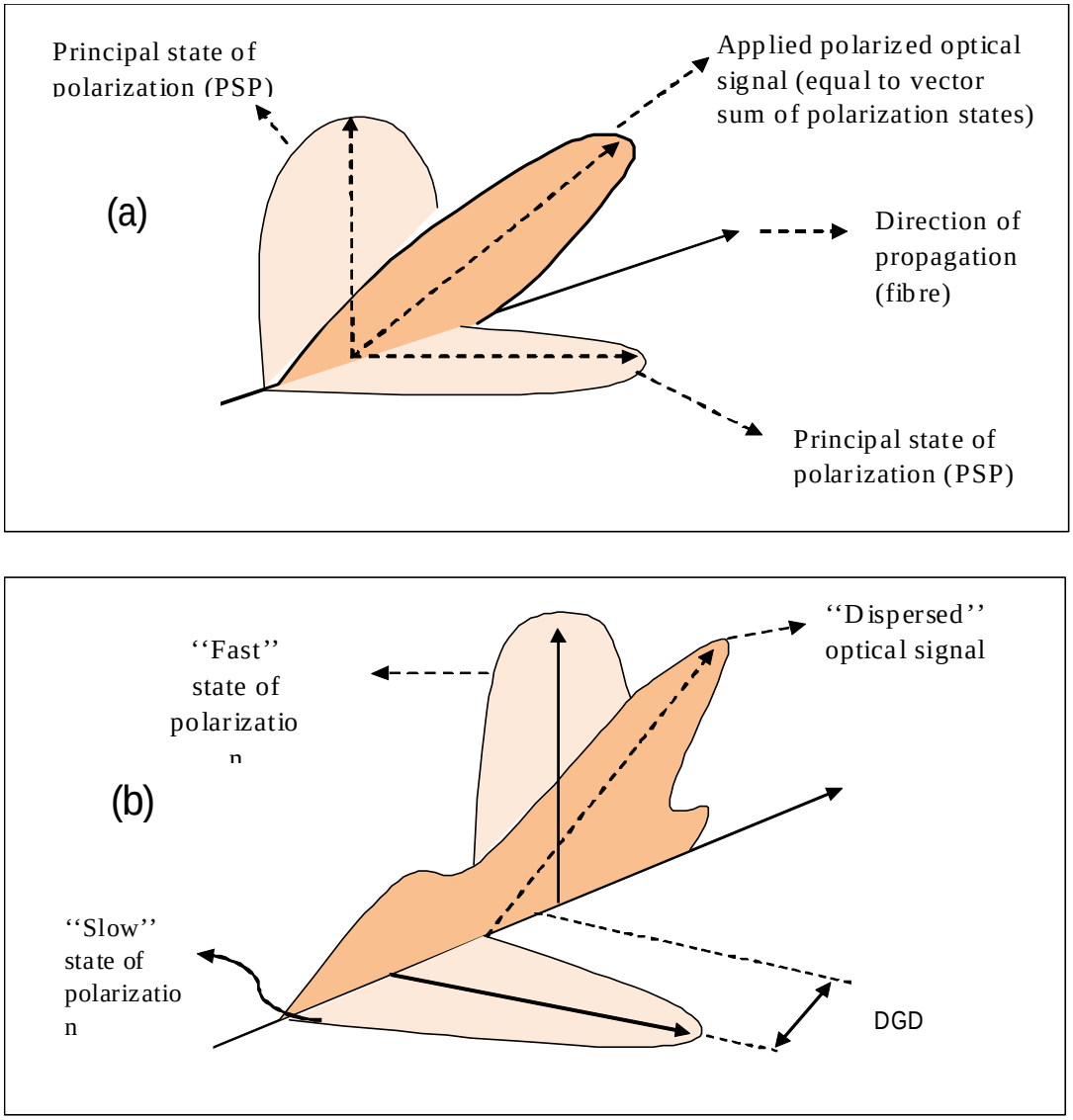

Fig. 2.7: Optical signal at (a) the input and (b) output of the fibre.

In other words, the PSP is defined as that input polarization for which the output state of polarization is independent of frequency to first order [20], i.e., over a small frequency range (bandwidth). It implies that any change of frequency within this bandwidth will

not change the output polarization. Therefore both the DGD and the PSPs are assumed to be frequency independent if only linear birefringence effect is being considered.

2.1.7 Linear Birefringence Vector

Based on the principal states model, the linear birefringence vector $\vec{\Omega}$ is defined as follows [21]:

$$\vec{\Omega} = \tau \vec{q} \quad \text{..... (2.9)}$$

where τ is the magnitude of the linear vector and is called the DGD, $\vec{q}$ is the unit Stokes vector pointing in the direction of the fast principal state of polarization in Stokes polarization space while $-\vec{q}$ points along the orthogonal slower axis. These orthogonal unit Stokes vectors are 180^0 apart. The input $\vec{\Omega}_{in}$, and output $\vec{\Omega}$, linear vectors for an optical fibre are related by $\vec{\Omega} = M\vec{\Omega}_{in}$, where M is Muller matrix. It can then be shown that angular frequency derivative of equation (2.9) will lead directly to the law of infinitesimal rotation, $\vec{S}_{out} = M\vec{S}_{in}$.

$$\left(\vec{S}_{out}\right)_{\omega} = \frac{d\vec{S}_{out}}{d\omega} = \vec{\Omega} \times \vec{S}_{out} \quad \text{..... (2.10)}$$

where $\Omega \times = M_{\omega} M^{T}$ and M^T is the transpose of M. This means that for a fixed input SOP, the output SOP, $\vec{S}_{out}$, will precess around $\vec{\Omega}$ as the angular frequency is changed.

The angle of precession is determined by the direction of $\vec{S}_{out}$ relative to $\vec{\Omega}$ while the rate at which $\vec{S}_{out}$ precesses around $\vec{\Omega}$ is determined by the magnitude, τ.

2.2 Nonlinear Effects in Optical Fibre

The response of any dielectric to light becomes nonlinear for intense electromagnetic fields, and optical fibres are no exception. On a fundamental level, the origin of nonlinear response is related to anharmonic motion of bound electrons under the influence of an applied field. This implies that the induced polarization will not be linear in the electric field anymore (harmonic approximation) but satisfies the more general relation:

$$P = \varepsilon_0(\chi^1 E \quad + \quad \chi^2 EE \quad + \quad \chi^3 EEE + ... \quad) \ldots\ldots\ldots\ldots\ldots\ldots \quad (2.11)$$

where E is the electric field, ε_0 the vacuum permittivity and $\chi^{(j)}$ the j-th order susceptibility at optical frequencies. The first term, $\chi^{(1)}$, describes the linear behavior of the system whereas the second term $\chi^{(2)}$ describes quadratic effects such as second harmonic generation and sum frequency generation. However, in glasses, because of the optical isotropy, the second-order susceptibility is zero unless the glass has been poled [6]. The third term $\chi^{(3)}$ is responsible for nonlinearities in the fibre and can result in nonlinear refraction (Kerr effect) given by [22]:

$$n' = n_0 + \underbrace{n_2 \frac{P}{A_{eff}}}_{\substack{nonlinear \\ contribution}} \quad \ldots\ldots\ldots\ldots\ldots\ldots\ldots\ldots\ldots\ldots\ldots\ldots \quad (2.12)$$

where n_0 is the linear refractive index, n_2 is the nonlinear-index coefficient, A_{eff} is the effective core area of the medium and P is the optical power inside the fibre. The intensity dependence of the refractive index leads to a large number of interesting nonlinear effects; the most widely studied due to their negative effect on the signal in a WDM system are self-phase modulation (SPM), cross-phase modulation (XPM) and four-wave mixing (FWM) [23].

2.2.1 The Coupled Nonlinear Schrodinger Equations

Based on [23], the propagation equations for the two principal polarizations in birefringent media can be obtained by factoring out the transverse dependence of the electric field components E_x and E_y:

$$E(r,t) = H(x,y)A(z,t)\exp(i\beta_0 z) \quad \text{..... (2.13)}$$

where H describes the spatial distribution of the single fibre mode, A is the (slowly varying) amplitude envelope and β_0 is the propagation constant. Making allowance for PMD (including polarization mode coupling) and polarization dependent loss (PDL), the slowly varying amplitudes, A_x and A_y, are described well by the following set of two coupled stochastic nonlinear Schrödinger equations [24]:

$$\frac{\partial A_x}{\partial z} + \beta_{1x}\frac{\partial A_x}{\partial t} + \frac{i\beta_2}{2}\frac{\partial^2 A_x}{\partial t^2} + \frac{\alpha_x}{2}A_x - \frac{\beta_3}{6}\frac{\partial^3 A_x}{\partial t^3} + i\kappa(z)A_y e^{-i\Delta\beta_0 z}$$

$$= i\gamma\left(|A_x|^2 + \frac{2}{3}|A_y|^2\right)A_x + \frac{i\gamma}{3}A_x^* A_y^2 e^{-2i\Delta B_0 z} \quad \text{..... (2.14a)}$$

$$\frac{\partial A_y}{\partial z}+\beta_{1y}\frac{\partial A_y}{\partial t}+\frac{i\beta_2}{2}\frac{\partial^2 A_y}{\partial t^2}+\frac{\alpha_y}{2}A_y-\frac{\beta_3}{6}\frac{\partial^3 A_y}{\partial t^3}-i\kappa^*(z)A_x e^{+\mathrm{i}\Delta\beta_0 z}$$

$$=\mathrm{i}\gamma\left(\left|A_y\right|^2+\frac{2}{3}\left|A_x\right|^2\right)A_y+\frac{\mathrm{i}\gamma}{3}A_y^* A_x^2 e^{+2\mathrm{i}\Delta B_0 z} \quad \text{…….…. (2.14b)}$$

where $\kappa(z)$ is the random mode coupling coefficient, $\Delta\beta_0$ is the birefringence parameter, α_x and α_y are the losses for the two polarization modes and the nonlinear parameter γ is given by:

$$\gamma=\frac{2\pi}{\lambda}\frac{n_2}{A_{eff}} \quad \text{……..……...…. (2.15)}$$

The average loss is given by $\alpha = (\alpha_x + \alpha_y)/2$, while $\Delta\alpha = \alpha_x - \alpha_y$ represents the polarization dependent loss (PDL) in the link. The last term on the right-hand side of Eq. (2.14) is due to coherent coupling between the polarization components and leads to degenerate Four-Wave Mixing (FWM). However, if the fibre length $L >> L_B$ from Eq. (2.8) in subsection 2.1.4, chapter 2, such as is considered here, it changes signs often and averages out to zero and therefore it can be neglected.

If it is assumed that the fibre is linearly birefringent then mode coupling, PDL and third-order dispersion β_3 can be neglected since β_2 is not equal to zero. The reduced equations now become:

$$\frac{\partial A_x}{\partial z}+\beta_{1x}\frac{\partial A_x}{\partial t}+\frac{i\beta_2}{2}\frac{\partial^2 A_x}{\partial t^2}+\frac{\alpha}{2}A_x=\mathrm{i}\gamma\left(\left|A_x\right|^2+\frac{2}{3}\left|A_y\right|^2\right)A_x \quad \text{…….. (2.16a)}$$

$$\frac{\partial A_y}{\partial z}+\beta_{1y}\frac{\partial A_y}{\partial t}+\frac{i\beta_2}{2}\frac{\partial^2 A_y}{\partial t^2}+\frac{\alpha_y}{2}A_y=\mathrm{i}\gamma\left(\left|\mathrm{A_y}\right|^2+\frac{2}{3}\left|\mathrm{A_x}\right|^2\right)\mathrm{A_y} \quad \text{…..... (2.16b)}$$

The first term on the right-hand side in the brackets represents the self-phase modulation (SPM). The second term represents the cross-phase modulation (XPM).

2.2.2 Self Phase Modulation (SPM)

In SPM, the intensity modulation of an optical beam results in the modulation of its own phase via modulation of the refractive index of the medium. The resulting time-dependent change, or modulation of the phase, leads to spectral broadening or frequency chirping [25].

$$\Delta\omega(z,t) = -\frac{\partial\varphi_{NL}}{\partial t} = -\frac{2\pi n_2}{\lambda A_{eff}}\frac{d\,P(t)}{dt}z = -n_2\frac{d\,I(t)}{dt}kz \quad \text{..... (2.17)}$$

where I is the optical intensity, k and φ_{NL} the wavevector and nonlinear phase shift, respectively. Because of the time derivative in Eq. (2.17), it is clear that SPM is essentially a pulse effect, with the leading edge of the pulse being red-shifted and the trailing edge blue-shifted. In addition, the pulse spectrum exhibits characteristic oscillations, which are due to the interference, within the pulse, of component waves with the same frequency but different phases. The nonlinear spectral broadening can be either compensated or magnified by the chromatic dispersion of the fibre. In the normal chromatic-dispersion regime ($\lambda < \lambda_{ZDW}$), in which red light travels faster than blue light, the nonlinear dispersion is magnified by the chromatic dispersion, resulting in enhanced broadening. In the anomalous dispersion regime ($\lambda > \lambda_{ZDW}$), the nonlinear dispersion is compensated, leading to pulse compression or, when exactly balanced, to the formation of solitons [26].

The net effects of SPM depend essentially on the characteristics of the initial pulse, its temporal shape, spectrum, and initial chirp, to which one must add the effect of chromatic dispersion. The shorter the pulse, the shorter the dispersion length L_D, and the more important group velocity dispersion (GVD) becomes. With appropriate dispersion and pulse characteristics, SPM can be used for the spectral and temporal compression of pulses, soliton generation and pulse regeneration.

2.2.3 Cross-Phase Modulation (XPM):

Cross-phase modulation is a similar effect to SPM, but it involves two optical beams instead of one [27]. In XPM, the intensity modulation of one of the beams results in a phase modulation of the other. As in SPM, the phase modulation translates into a frequency modulation that broadens the spectrum. However, because the total intensity is the square of a sum of two electric-field amplitudes, the spectral broadening caused by XPM is twice as large as in SPM.

$$n = n_0 + n_2\left|E_1 + E_2\right|^2$$

$$\Rightarrow \varphi_{NL}^{\omega 1}(z) = \frac{2\pi n_2}{\lambda A_{eff}}\left[\left|E_1\right|^2 + 2\left|E_2\right|^2\right] \text{.....} \quad (2.18)$$

In the expression for the nonlinear phase shift in Eq. (2.18), the presence of two terms shows that XPM (second term) is always accompanied by SPM (first term). A similar expression can be written for the second beam $\varphi_{NL}^{\omega 2}(z)$. If one of the two beams (the pump) is much stronger than the other (the probe or signal), XPM will primarily act from that pump beam to the weaker signal beam. Because it is a nonlinear effect

resulting from a two-beam interaction, XPM can be used for a number of all-optical applications in communication networks: wavelength conversion, demultiplexing, switching [28], and other optical-control applications.

However, XPM can create significant problems in WDM communication networks because of the crosstalk it can induce between nearby channels [29]. This can affect the pulse shapes and amplitudes in different channels and lead to the time-dependent depolarization of nearby channels [30]. When taking polarization into consideration, an array of new nonlinear effects can be predicted and are indeed observed in fibres. As should be expected, these effects depend intimately on the particular birefringence characteristics of the fibre and on the SOP of the optical wave(s). This birefringence can be intrinsic to the fibre, but it can also be induced by optical nonlinearities. The nonlinear contributions to birefringence are given by [31].

$$\Delta n_x = n_2\left(\left|E_x\right|^2 + \frac{2}{3}\left|E_y\right|^2\right) \text{ and } \Delta n_y = n_2\left(\left|E_y\right|^2 + \frac{2}{3}\left|E_x\right|^2\right) \text{..... (2.19)}$$

where n_2 is the nonlinear parameter defined earlier. From equation (2.19), it is easy to see that the nonlinear birefringence and related effects must depend on the relative optical intensities in the *x* and *y* direction. These two components interact nonlinearly in a way that is analogous to XPM, resulting in a relative nonlinear phase shift between the two components [31]:

$$\Delta\varphi_{NL} = \gamma L_{eff}\left(1 - B\right)\left(P_x - P_y\right) \text{..... (2.20)}$$

where $P_{x,y}$ are the powers in the *x* and *y* components, respectively, and *B* describes the ellipticity of the fibre (*B* = 2⁄3 for a linearly birefringent fibre). Such a relative nonlinear

phase shift can be introduced by co-propagating a strong pump, polarized along the *x*-axis of the fibre, along with a weak arbitrarily polarized signal. $\Delta\varphi_{NL}$ then determines the particular evolution of the polarization as the beam propagates and can, for instance, lead to a rotation of the polarization (optical Kerr effect) [32]. When taking the respective polarization of the two beams into account, XPM can also give rise to interesting temporal and spectral polarization effects. In a pump-probe situation, the probe polarization can be shown to rotate, with different parts of the pulse developing different SOP [32].

2.2.4 Four-Wave Mixing (FWM)

FWM is a parametric process, in which three optical fields, propagating at different frequencies (non- degenerate case) in the same direction along a fibre, producing a fourth field, propagating in the same direction, which drains power from the originating three fields. If three intense lightwaves of different frequencies (ω_i, ω_j, ω_k) are input to an optical fibre, additional frequencies are generated through the four-wave mixing (FWM) process and the generated fourth signal is given by [33].

$$\omega_{ijk} = \omega_i + \omega_j - \omega_k \quad \text{.....} \quad (2.21)$$

with $i,j \neq k$.

In every WDM system, it is important to eliminate the effect of four-wave mixing because it induces channel crosstalk which limits the capacity of WDM trans-mission, particulary over optical dispersion shifted fibres (DSF). From [34], it was observed that when all the lasers were modulated, crosstalk was observed at all frequencies between

the two adjacent channels. It was concluded that FWM crosstalk becomes significant when the signal powers exceed 0 dBm/channel in a 10 GHz spaced, 100-channel system using 1.5-pm sources and a single-mode fibre. Thus, the successful design of high-capacity orthogonal frequency-division multiplexing (OFDM) systems must include careful consideration of possible FWM interactions in the transmission fibre. Since the dispersion-shifted fibre is no longer being used for data transmission, FWM is not much of an issue in communication systems.

2.3 Nonlinear Polarization Evolution in Birefringent Fibre

The nonlinear interaction in WDM systems induces a nonlinear polarization scattering in one optical channel whenever there is high optical power present in the other channel. This leads to a power dependent change of the state of polarization. When analyzing nonlinear polarization evolution, two co-propagating channels are considered having arbitrary polarization. If the slowly varying envelopes of the fields for the two channels are denote by $\vec{A}_a$ and $\vec{A}_b$, their evolution in the fibre can be described by the equation [35]:

$$-i\frac{\partial \vec{A}_a}{\partial z} = \frac{8}{9}\gamma\left\{\left(\vec{A}_a^{+}\mapsto \vec{A}_a\right)\vec{A}_a + \left(\vec{A}_b^{+}\mapsto \vec{A}_b\right)\vec{A}_a + \left(\vec{A}_b^{+}\mapsto \vec{A}_a\right)\vec{A}_b\right\} \quad \text{..... (2.22)}$$

where $\vec{A}^{+}$ is the transpose of *A*.

By neglecting polarization mode dispersion (PMD) and polarization dependent loss (PDL), it can also be shown that no polarization evolution takes place between orthogonally polarized signals. This can be understood from [35] which showed that the

rate of change of Stokes vectors $\vec{S}_a$ and $\vec{S}_b$ of the two channels along the z-axis is given by:

$$\frac{\partial \vec{S_a}}{\partial z} = \frac{16}{9}\gamma P_o\left(\vec{S}_a \times \vec{S}_0\right) \text{ and } \frac{\partial \vec{S_b}}{\partial z} = \frac{16}{9}\gamma P_o\left(\vec{S}_b \times \vec{S}_0\right) \text{..... (2.23)}$$

where $\vec{S}_a$ and $\vec{S}_b$ represent the Stokes vectors of the two channels, P_0 is the optical power, and the average vector of $\vec{S}_a$ and $\vec{S}_b$, is $\vec{S}_0 = \frac{1}{2}\left(\vec{S}_a + \vec{S}_b\right)$. Equation (2.23) indicates that the Stokes vectors of two signals rotate at the same rate about the vector $\vec{S}_0$.

The magnitude of the vector $\vec{S}_0(P_m)$ depends on the fixed relative polarization angle θ between the probe and pump and the peak powers of probe (P_s) and the pump (P_p), respectively, according to the equation [36]:

$$P_m = \sqrt{P_s{}^2 + P_p{}^2 + 2P_sP_p\cos\theta} \text{ ..... (2.24)}$$

According to Eq. (2.24), the channel with the dominant power remains fixed, since its Stokes vector is almost coincident with $\vec{S}_0$. Therefore the output Stoke vector of the probe channel is guided by the relative angles between the pump and probe input SOP vectors and the magnitude of the pump power. The probe signal is highly depolarized if the input pump power is high and also if the input SOP vectors of the pump and probe are perpendicular to one another in Jones space. But the signal remains polarized if the input SOP vectors are anti-parallel or parallel, regardless of the input pump power. This is demonstrated in the results discussed in section 4.0.

Since the linear SOPs rotate around S_1 while the nonlinear SOPs rotate around S_3, it would be interesting to explore how the linear and nonlinear effects influence the state of polarization evolution.

2.4 Interaction of Linear and Nonlinear Polarization Rotation

At low intensities, the linear birefringence causes polarization fluctuations which produce linear signal pulse distortion known as linear PMD. However, as the distance of transmission continues to increase, the signals carrying high intensities also need to increase in order to reduce the number of repeaters and amplifiers along the link. Under these conditions, in addition to linear birefringence, the intensity induced-birefringence known as *nonlinear birefringence* is developed in the fibre. The power dependent polarization fluctuation is produced causing the intensity dependent signal pulse distortion known as *nonlinear* PMD [37]. Thus, the nonlinear PMD exists whenever there is high intensity carried by the signals and its effect will affect very high data rate systems operating at near 100 Gb/s [38]. Also, from [38] it was stated that reducing the linear effects by decreasing the decorrelation length reduces the rate of mixing on the Poincaré sphere which in turn increases the nonlinear effects.

The numerical study of the coupling between linear orthogonal modes due to nonlinear polarization evolution has been carried out where it was concluded that the interaction between the linear and nonlinear birefringence causes the successive and periodic energy exchange between the fast and slow linear modes of the fibre [39]. Models have

been developed that describe the interaction between XPM, PMD and PDL [40]. It showed that XPM changes the direction of the polarization but does not affect the DGD.

2.5 Fibre Optic Sensor

The field of measurement and instrumentation, particularly sensor development, is one that has expanded rapidly in recent years. The need for high quality sensors to be integrated into sophisticated measurement and control system is clear. In parallel with rapid advance in development of sensors based on microelectronics, those based on optical techniques have expanded significantly over last few years and have found many applications in the industrial field. This is because, compared with other types of sensors, fibre optic sensors have several advantages such as small size and weight, immunity to electromagnetic interferences, large bandwidth and hence offers possibility of high multiplexing potentials, intrinsically safe in explosive environments, highly reliable and secure with no risk of fire, high sensitivity and accuracy [41], just to mention but a few. Fibre optic sensors (FOS) can be used for the measurement of many physical or chemical properties [42]. The principle is based on the fact that light in an optical fibre can be modified in response to an external physical, chemical, biological, biomedical or similar influence. Most properties can be detected with fibre optic sensors such as strain, pressure, sound, displacement (position), temperature, magnetic field, electric field, chemical analysis, liquid level, rotation, radiation, vibration, among others.

2.5.1 Classification of Fibre Optic Sensors

Fibre optic sensors can be specified in terms of the types of perturbation or the principle of operation. Thus, they can be described by the chemical concentration, strain, temperature, stress or the other physical measurand. The operating principle can be based on variations of intensity, phase, polarization and wavelength [42]. Extrinsic or intrinsic sensors are another classification scheme. In the former, sensing takes place in a region outside the fibre and the fibre essentially serves as a conduit for the to-and-fro transmission of light to the sensing region in an efficient and desired form. On the other hand, in an intrinsic sensor one or more of the physical properties of the fibre undergo a change. Fibre optic sensors can also be classified in response to their measurements points. The three important classes here are; point to point sensors, multiplex sensors and distributed sensors. In point to point type there is a single measurement point at the end of the fibre optic connection cable, similar to most electrical sensors. Multiplexed sensors allow the measurement at multiple points along a single fibre line and distributed sensors are able to sense at any point along a single fibre line, typically every meter over many kilometers of length [43].

More commonly, fibre optic sensors (FOS) can be divided into two basic categories: Intensity based sensors and interferometric-based sensors. Generally, intensity modulated FOS are related to the displacement or some other physical perturbation that interacts with the fibre. The perturbation induces light intensity change at the detector. Interferometric-based FOS commonly compare the phase of light in a sensing fibre to a reference fibre in an interferometer. They are much more accurate and

sensitive than intensity-based sensors because the phase of light wave propagating in an optical fibre is more sensitive to external influences than any other parameter [44] and as such, they can be used over a much larger dynamic range. However, since optical phase change cannot be directly detected (optical waves have frequencies in the range of few hundred THz), they require much more complex signal processing techniques which make them expensive.

2.5.2 Intensity-based Fibre Optic Sensor

Intensity-based sensors measure the optical intensity as a function of the perturbing environment, as shown in Fig. 2.8 below. The change of the optical intensity can be related to transmission, reflection, microbending, or other phenomena such as absorption, scattering, or fluorescence. Intensity-based fibre optic sensors can be divided into reflection sensors, transmission sensors, and microbending sensors.

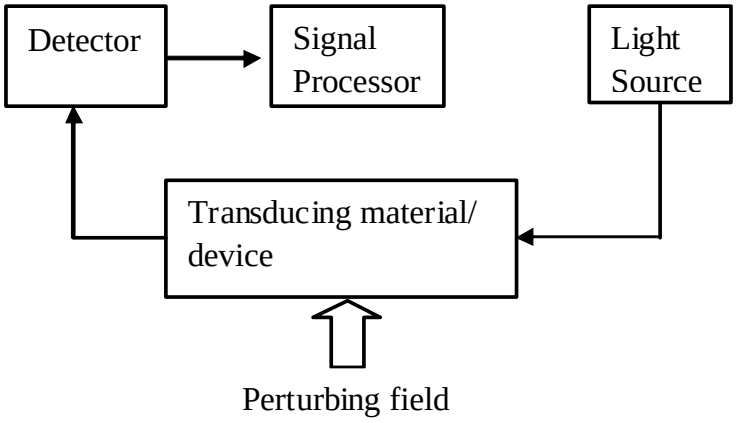

Fig. 2.8: Intensity-based sensor.

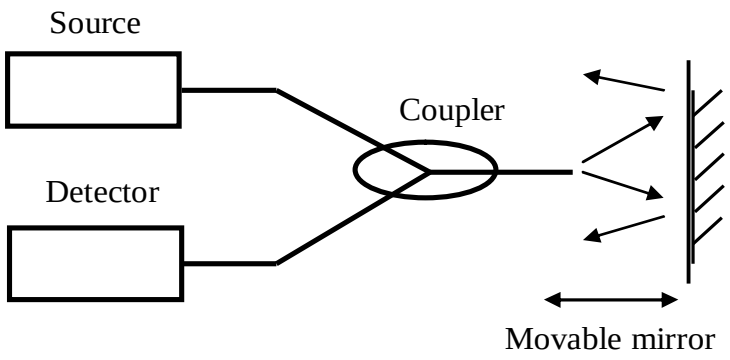

Fig. 2.9: Fibre optic sensor using reflection.

Figure 2.9 shows the basic principle of a fibre optic sensor using reflection. Light travels along the fibre from left to right, leaves the fibre end, and incidents on a movable reflector. If the reflectors move towards the fibre, most of the light can be reflected back into the fibre so that a high light intensity signal is detected. However, when the reflector moves away from the exit end of the fibre, less light is coupled back into the fibre, and so a weak signal is detected. Therefore, the monotonic relationship between fibre–reflector distance, and reflected light intensity can be used to measure the displacement distance. To avoid the influence of the intensity fluctuation of the light source, a suitable reference signal is usually added in this type of intensity-based fibre optic sensor.

The major problem associated with intensity sensors are random changes of transmissivity of optical path and variations of the output power of the optical source, which directly affects the accuracy of the sensor. Intensity sensors therefore need a mechanism that compensates for those changes.

2.5.3 Interferometric-based Fibre Optic Sensor

Interferometric-based sensors take advantage of interferometric techniques to measure pressure, temperature, rotation angle, magnetic field, e.t.c. Generally, the sensor uses a coherent laser source and two single mode fibres. The light is split and put into each fibre. If the environment perturbs one fibre relative to the other, a phase shift occurs that can be detected precisely. The shift of the phase is detected by an interferometer. There are four interferometric configurations: the Mach-Zehnder, the Michelson, the Fabry-Perot, and the Sagnac. Figure 2.10 shows the schematic of a Mach-Zehnder interferometer.

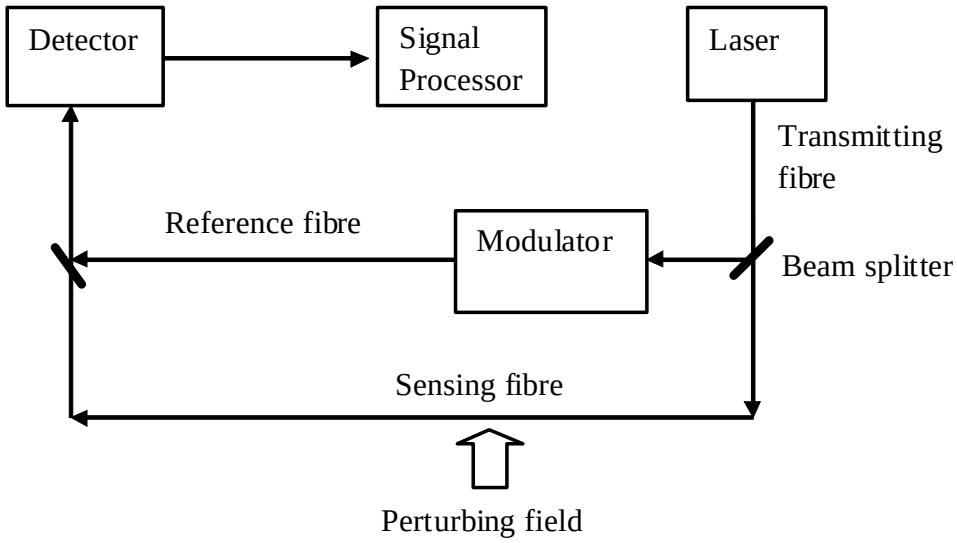

Fig. 2.10: Interferometric sensor (Mach-Zehnder interferometer).

The laser beam from the light source splits at the beam splitter so that light travels in the reference single mode fibre and the sensing fibre, which is exposed to the perturbing environment. If the light in the sensing fibre and the light in the reference fibre are exactly in phase after recombining, they constructively interfere and the output signal intensity is high. If they are out of phase, destructive interference happens and the

received optical intensity is lower. Such devices have a phase shift if the sensing fibre has a length or refractive index change, or both.

In the Fabry-Perot interferometer, a multiple-beam is used. Figure 2.11 shows a fibre optic Fabry-Perot interferometer. Due to the high reflectivity of the mirrors, in this type of interferometer the light bounces back and forth in the cavity many times, increasing the phase delay many times. The transmitted output intensity of the Fabry–Perot interferometer is given by the fact that the higher the reflection coefficient (F_c), the sharper the interference peak will be. In other words, near the peak region, the output light intensity is very sensitive to the small change in the phase delay.

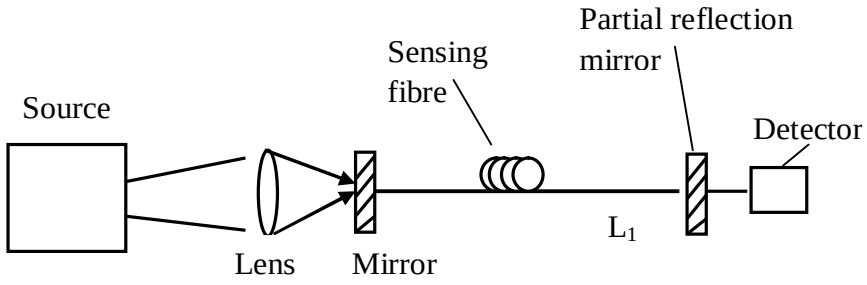

Fig. 2.11: Fabry-Perot interferometer-based fibre optic sensor.

The larger the F_c number, the sharper the interference peak will be. Thus, the sensitivity of a Fabry-Perot interferometer-based fibre sensor can be much higher than that of the Mach-Zehnder or Michelson interferometer [45].

In summary, fibre optic interferometric sensors usually have the advantage such as the design flexibility, the large dynamic range and high resolution. However, because of the

nonlinear periodic characteristic of the interference signal, the accurate detection of the differential phase change of an interferometer turns to be a real challenge.

2.5.4 Polarization-based Fibre Optic Sensor

Inspite of many advantages, there is a growing demand for improved sensitivity, reliability, accuracy, flexibility and better compatibility of fibre optic sensors for various applications. Among the various optical sensor designs, polarimetric fibre optic sensor (PFOS) has its unique advantages over the rest [46]. When a force is applied along the length of a polarimetric fibre, an additional birefringence is introduced due to the elasto-optic effect i.e. the change in refractive index due to the applied force and is given by:

$$\Delta n = C_B F \quad \text{……...……...…..} \quad (2.25)$$

where C_B is Brewster constant and F is the applied force. In addition, in many cases, the stress or strain in different directions is different, so that the induced refractive index change is also different in different directions. Thus, there is an induced phase difference between different polarization directions. In other words, under the external perturbation, such as stress or strain, the optical fibre works like a linear retarder. Therefore, by detecting the change in the output polarization state, the external perturbation can be sensed [43]. To make the fibre optic sensor practical, it is necessary to display sensitivity to the phenomenon designed to measure insensitivity to changes in other environmental parameters. For the strain or stress measurement, environmental temperature is unwanted external parameter. For PFOS, environmentally induced refractive index changes in the two polarization directions are almost the same. Thus,

there is almost no induced phase difference between two polarization states and environmental temperature fluctuation will not substantially deteriorate the sensor's performance.

In this research, PFOS utilize the concept of nonlinear polarization coupling where the pump and the probe signals interact and only the probe signal is filtered out for analysis. The pump-probe scheme uses the three operating principles of FOS (intensity, phase and polarization) as will be seen in the results in chapter 4. Though, a number of sensors have been developed based on the effect of polarization coupling between two orthogonally polarized eigenmodes of polarization maintaining fibre [47, 48], few have been designed based on this scheme. From equation (2.23) in section 2.3, the Stokes' vectors $\vec{S}_a$ and $\vec{S}_b$ for the two channels perform a rotation around a time- and *z*-independent pivot $\vec{S}_0$. At coordinate *z*, the rotation angle is [49]

$$\psi(z) = \frac{8}{9}\gamma P_m \int_0^z e^{-\alpha z'} \, p\left(t - d_{sp} z'\right) dz' \quad \text{..... (2.26)}$$

and depends on the section of the pump bits that have walked past the probe from the input to coordinate *z*, as expressed by the *normalized* pump power $p\left(t - d_{sp} z'\right)$ in the above integral. The length over which the pump walks past the probe by one bit is known as walk off length ($L_\omega = T/d_{sp}$) where T is the bit time and d_{sp} is walk-off parameter. The magnitude of the pivot P_m is given by Eq. (2.24) and the rotation speed in Eq. (2.26) decreases in *z* because of the fibre attenuation α. It should be noted that the

rotation angle does not depend on the channel spacing between the pump and probe: no matter how far apart, the two CW channels undergo the rotation given in Eq. (2.26).

At the fibre output $z = L$ the SOP of the probe depicts in time a circular trajectory around the pivot, with a rotation angle that swings around an average value $\langle \psi(L,t) \rangle$ by an amount $\Delta\psi(L,t) = \psi(L,t) - \langle \psi(L,t) \rangle$, whose expression is obtained from (2.26). Without loss of generality, a reference frame of the Stokes' space in which the pivot is aligned with the third Stokes' axis S_3 is chosen, and the component of the average probe output SOP along S_2 is zero, so that the time-dependent output probe SOP is expressed as:

$$\hat{s}(L,t) = \frac{\vec{s}(L,t)}{P_s} = \begin{bmatrix} \sin\theta_s \cos\Delta\psi(L,t) \\ \sin\theta_s \sin\Delta\psi(L,t) \\ \cos\theta_s \end{bmatrix} \text{..... (2.27)}$$

where the zero-mean process $\Delta\psi(L,t)$ represents the SOP's azimuth, and θ_s is the angle between the probe and the pivot. Such an angle can be obtained from θ and the pump-probe power ratio PR = (P_p/P_s) through the analytical relationship $\theta_s = \theta - \arctan((\sin\theta)/(PR+\cos\theta))$. Using equation (2.27) in the definition of DOP yields

$$DOP = \sqrt{1 - \sin^2\theta_s \left[1 - \langle \cos\Delta\psi(t) \rangle^2 - \langle \sin\Delta\psi(t) \rangle^2 \right]} \text{..... (2.28)}$$

where all that is needed is evaluation of the time averages $\langle \cos\Delta\psi(t) \rangle$ and $\langle \sin\Delta\psi(t) \rangle$. Already, some conclusions can be drawn from such equations. First, the larger the swing angle, the smaller the DOP. Next, if pump and probe Stokes' vectors are initially aligned or counter-aligned, then $\sin\theta_s = 0$, so that the DOP is unity. Unfortunately, the

presence of polarization mode dispersion (PMD) prevents such initial alignment to be kept during propagation, so that depolarization occurs. The effect of PMD can be understood as follows. If the real fibre is assumed as a concatenation of randomly oriented birefringent plates, then within each plate, pump and probe rotate by different angles around the local birefringence vector. Hence, the net effect of PMD is to randomly vary the relative polarization angle θ and the orientation of the pivot $\vec{S}_0$ during propagation.

To evaluate the time-averages in Eq. (2.28), $\langle \cos \Delta\psi(t) \rangle$ and $\langle \sin \Delta\psi(t) \rangle$ are expanded in Fourier series as

$$\begin{aligned} \cos \Delta\psi(t) &= \cos\left[\Delta\psi_0 \sin(\omega_0 t + \varphi_0)\right] \\ &= J_0(\Delta\psi_0) + 2\sum_{n=1}^{+\infty} J_{2n}(\Delta\psi_0) \cos\left[2n(\omega_0 t + \varphi_0)\right] \\ \sin \Delta\psi(t) &= \sin\left[\Delta\psi_0 \sin(\omega_0 t + \varphi_0)\right] \\ &= 2\sum_{n=1}^{+\infty} J_{2n+1}(\Delta\psi_0) \sin\left[2n+1(\omega_0 t + \varphi_0)\right] \end{aligned} \quad \text{……..…….. (2.29)}$$

where $J_n(.)$ is the Bessel function of the first kind of order *n*. By averaging over a time much longer than 2T, one gets [50]

$$\langle \sin \Delta\psi(t) \rangle = 0 \ , \ \langle \cos \Delta\psi(t) \rangle = J_0(\Delta\psi_0) = J_0\left(\frac{\frac{8}{9}\gamma P_m}{\sqrt{\alpha^2 + \left(\frac{\pi}{L_\omega}\right)^2}} \right) \text{……...…. (2.30)}$$

Now using equation 2.30 in 2.28 gives:

$$DOP = \sqrt{1-\sin^2\theta_S\left\{1-\left[\langle\cos\Delta\psi(t)\rangle\right]^2\right\}} \quad \text{(2.31)}$$

where the dependence of the DOP on the relative pump-probe polarization angle θ is implicit in θ_s and P_m. From equations (2.30) and (2.31) it can be concluded that, if polarization control of the signals ($\theta = \theta_s = 0$ or $\theta = \theta_s = \pi$) cannot be achieved due to PMD, the basic countermeasure against DOP degradation is to increase the bit walk-off by further spacing the channels or by using a more dispersive fibre, so as to reduce the argument of the Bessel function. Clearly, also increasing the bit rate implies a reduction of XPM-induced DOP degradation.

2.6 Split-Step Fourier Method

It is required to solve the nonlinear Schrödinger equation to understand various impairments occurring during signal transmission. However, it is not possible to solve it analytically when both the nonlinearity and the dispersion effect are present, except in the very special case of soliton transmission. Therefore, numerous numerical algorithms have been developed to solve Eqs. (2.14) or (2.16). The split-*step Fourier method* is one of them, and is the most popular algorithm because of its good accuracy and relatively modest computing cost [51] compared with most finite difference schemes. The algorithm is briefly discussed in the following. Equation (2.16) can be expressed as:

$$\frac{\partial A}{\partial z} = \left(\hat{L} + \hat{N}\right)A \quad \text{(2.32)}$$

where the linear operator, $\hat{L} = -\frac{\alpha}{2} - \frac{i\beta_2}{2}\frac{\partial^2}{\partial t^2}$ and the nonlinear operator, $\hat{N} = i\gamma|A(z,t)|^2$.

When the electric field envelope, $A(z, t)$, has propagated from z to $z+\Delta z$, the analytical solution of Eq.(2.32) will be of the form:

$$A(z+\Delta z,t) = \exp(\Delta z(\hat{L}+\hat{N}))A(z,t) \quad \text{..... (2.33)}$$

In the split-step Fourier method, it is assumed that the two operators commute with each other. That is,

$$A(z+\Delta z,t) \approx \exp(\Delta z\hat{L}) \exp(\Delta z\hat{N})A(z,t) \quad \text{..... (2.34)}$$

Equation (2.34) suggests that $A(z+\Delta z,t)$ can be estimated by applying the two operators independently. The exponential operator $\exp(\Delta z \hat{L})$ can be evaluated in the Fourier domain using the prescription:

$$\exp(\Delta \hat{L})B(z,t) = F_t^{-1}\exp\left[\Delta z \hat{L}(i\omega)\right]F_t B(z,t) \quad \text{..... (2.35)}$$

where F_t denotes the Fourier-transform operation, $\hat{L}(i\omega)$ is obtained from operator $\hat{L}$ by replacing the differential operator $\frac{\partial}{\partial t}$ by $i\omega$ and ω is the frequency in the Fourier domain. As $\hat{L}(i\omega)$ is just a number in the Fourier space, the evaluation of Eq. (2.35) is straightforward. The use of the Fast Fourier Transform (FFT) algorithm makes numerical evaluation of Eq. (2.35) relatively fast. It is for this reason that the split-step Fourier method can be faster by up to two orders of magnitude compared with most finite-difference schemes.

The simulation time of Eq. (2.34) will greatly depend on the size of Δz. To reduce simulation time, a more refined algorithm, the so called *symmetrized split-step Fourier*

method, was devised [23]. Mathematically, the symmetrized split-step Fourier method can be expressed as follows:

$$A(z+\Delta z,t) \approx \exp\left(\frac{\Delta z}{2}\hat{L}\right)\exp\left(\int_z^{z+\Delta z}\hat{N}(z')dz'\right)\exp\left(\frac{\Delta z}{2}\hat{L}\right)A(z,t) \quad \text{..... (2.36)}$$

While Eq. (2.34) assumes that nonlinearities are lumped at every Δz, Eq. (2.36) assumes the nonlinearities are distributed through Δz, which is more realistic. Because of the symmetric form of the exponential operators in Eq. (2.36), this scheme is known as the symmetrized split-step Fourier method. The integral in the middle exponential is useful to include the z dependence of the nonlinear operator $\hat{N}$. When Δz is sufficiently small, the evaluation of the nonlinear operator is approximated as:

$$\int_z^{z+\Delta z}\hat{N}(z')dz' \approx \frac{\Delta z}{2}\left[\hat{N}(z)+\hat{N}(z+\Delta z)\right] \quad \text{..... (2.37)}$$

However, Eq. (2.37) requires iterative evaluation because $\hat{N}(z+\Delta z)$ is not known at $z+\Delta z/2$. Initially, $\hat{N}(z+\Delta z)$ will be assumed to be the same as $\hat{N}(z)$. Although the iterative evaluation is time-consuming, the improved numerical algorithm allows the use of larger Δz than that of Eq. (2.34), which will result in saving overall computational time.

The implementation of the split-step Fourier method is relatively straightforward. The fibre length is divided into a large number of segments that need not be spaced equally. The optical pulse is propagated from segment to segment using the prescription of Eq. (2.36). More specifically, the optical field $A(z,t)$ is first propagated for a distance $\Delta z/2$

with dispersion only using the FFT algorithm in Eq. (2.35). At the midplane $z+\Delta z/2$ the field is multiplied by a nonlinear term that represents the effect of nonlinearity over the whole segment length Δz. Finally, the field is propagated in the remaining distance $\Delta z/2$ with dispersion only to obtain $A(z+\Delta z,t)$. In effect, the nonlinearity is assumed to be lumped at the midplane of each segment.

In the implementation of SSFM, it is required that step sizes in z and t be selected carefully to maintain the required accuracy. In particular, it is necessary to monitor the accuracy by calculating the conserved quantities such as the pulse energy (in the absence of absorption) along the fibre length. The optimum choice of step sizes depends on the complexity of the problem. Although a few guidelines are available [52, 53], it may sometimes be necessary to repeat the calculation by reducing the step size to ensure the accuracy of numerical simulations. The time window should be wide enough to ensure that the pulse energy remains confined within the window. Typically, window size is 10–20 times the pulse width. In some problems, part of the pulse energy may spread so rapidly that it may be difficult to prevent it from hitting the window boundary. This can lead to numerical instabilities as the energy reaching one edge of the window automatically re-enters from the other edge (the use of the FFT algorithm implies periodic boundary conditions). It is common to use an “absorbing window” in which the radiation reaching window edges is artificially absorbed even though such an implementation does not preserve the pulse energy.

The name SSFM arises for two reasons. First, the method relies on computing the solution in small steps, and treating the linear and the nonlinear steps separately. Second, it is necessary to Fourier transform back and forth because the linear step is made in the frequency domain while the nonlinear step is made in the time domain. This makes the technique superior to the course step method. The Coupled Nonlinear Schrodinger Equation (C-NLSE) is generally numerically integrated by the SSFM, as shown schematically in Fig. 2.12. Generally, the split-step Fourier method is a powerful tool provided care is taken to ensure that it is used properly.

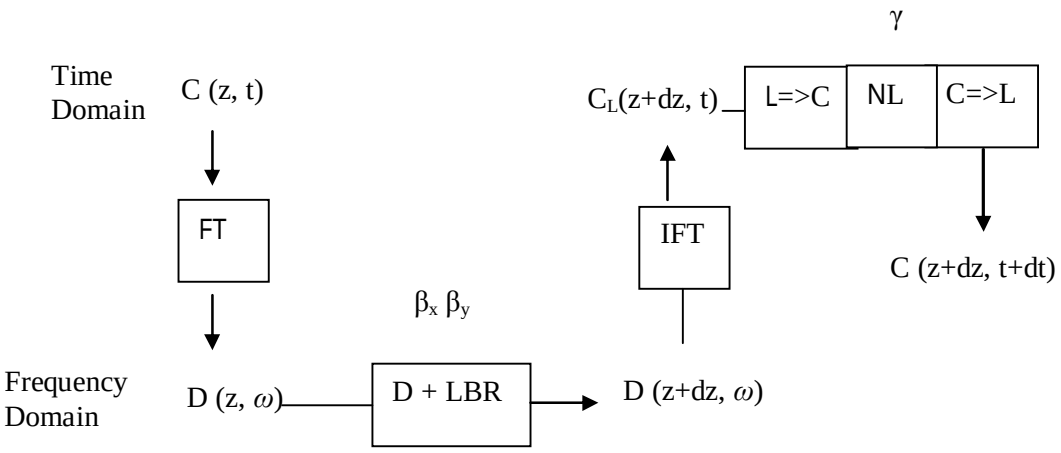

Fig. 2.12: Schematic representation of the structure of the SSFM algorithm in one fibre segment.

where D-Dispersion, LBR-Linear birefringence, NL-nonlinearity, FT-Fourier transform, IFT-inverse Fourier transform, L=>C and C=>L indicate transformation from linear to a circular basis and vice versa, respectively [54].

CHAPTER 3

METHODOLOGY

3.1 Research Design

In this research, both experimental and simulation work was carried out. Two simulation packages Optiwave and Matlab were used in this study because both Optiwave and Matlab simulation tools employ pseudo-spectral numerical method (Split Step Fourier Method) to solve Coupled Nonlinear Schrodinger Equation (C-NLSE). The advantage of this method over other numerical methods is given in section 2.6. All the experimental work presented in this thesis was done in Optical Fibre Research Unit, Physics Department, Nelson Mandela Metropolitan University-Port Elizabeth, South Africa. The setup was as shown in Figure 3.1.

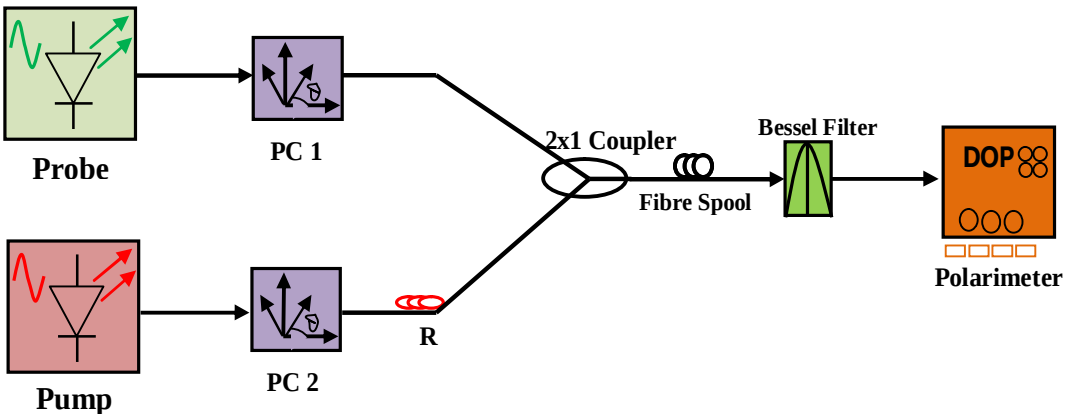

Fig. 3.1: A set up of a two-channel system (PC = polarization controller and R = sensing fibre used only for sensor set up)

Figure 3.1 shows the setup that was used for both experimental and simulation studies. A linearly polarized probe of input wavelength 1552.52 nm and a similarly polarized pump at input wavelength 1552.92 nm, giving a channel spacing of 50 GHz (0.4 nm)

both in the form of continuous waves, were coupled using a 2x1 coupler and co-propagated in a 1.7 km single mode fibre (SMF). The standard single mode fibre had linear PMD of 0.5 ps/$\sqrt{km}$, effective area of 80 μm^2 and a dispersion parameter of 17 ps/nm-km. The probe and the pump signals were provided by a wavelength division multiplexing (WDM) source. Polarization controller, PC1, maximized the probe input power into the fibre, while polarization controller, PC2, rotated the input pump SOPs with respect to the probe signal SOP. An optical filter of bandwidth 0.3 nm was used to filter out the probe signal and a polarimeter was used to monitor the DOP of the probe. The pump signal was launched at powers of 3 dBm and 13 dBm and for each input power the pump signal SOPs were rotated through 180^o while observing the output DOP of the probe (Fig. 4.3 see in the following chapter).

Also, simulation was done using a fibre of length 24 km which was modified into a concatenation of linearly birefringent trunks of constant length L_c to obtain different segments. As the input power of the pump signal was varied, the DOP and SOP angles of the probe were collected. The input probe power was kept constant. Using a similar set up as that used to generate data for Fig. 4.3, experimental work was done but using different channel spacing of 50 GHz, 100 GHz and 200 GHz where the DOP and SOP vectors of the probe were used as output indicators.

More simulations were done numerically using the Matlab tool, fibre of length 24 km was modeled as a concatenation of linearly birefringent trunks with length Lc = 100 m and random birefringence axis orientation. At a relatively high pump power and low

probe power, the output amplitude of the signal was measured over time at different values of modal birefringence $\Delta\beta_1$ and the corresponding Poincaré sphere representation given by plotting the SOPs on the sphere. Also, simulations were done where modal birefringence $\Delta\beta_1$ was kept constant and using higher pump power and low probe power the probe output signal was investigated over time.

For fibre optic sensor experiments, the external perturbation acted on the sensing fibre (R) in Fig. 3.1. For the design of stress sensor, polarization maintaining fibre (PMF) and large effective area fibre (LEAF) were used as sensing elements. The pump channel at R-section in Fig 3.1 was subjected to varying weights within the range of 2.5-32.5 kg while the output probe DOP measured.

In temperature sensing, (PMF) and single mode fibre (SMF) were used as sensing fibres. The sensing length was immersed in a jar containing water that was heated to approximately 100 ^{0}C and allowed to cool. A thermocouple was used to measure temperature as the DOP of the probe was monitored with decrease in temperature. In all the designs, the channel spacing between the pump and the probe was 50 GHz (0.4 nm). The experimental set up for the optical fibre sensors are given in appendix B.

CHAPTER 4

RESULTS AND DISCUSSION

4.1 Introduction

In this chapter the effects of linear and nonlinear birefringence are investigated. The interaction between the linear and nonlinear birefringence was also studied and the results discussed in detail in this chapter. This led to the possibility of designing a fibre optic sensor. The designed sensor was used to measure stress, strain and temperature.

4.2 Effect of Linear Birefringence

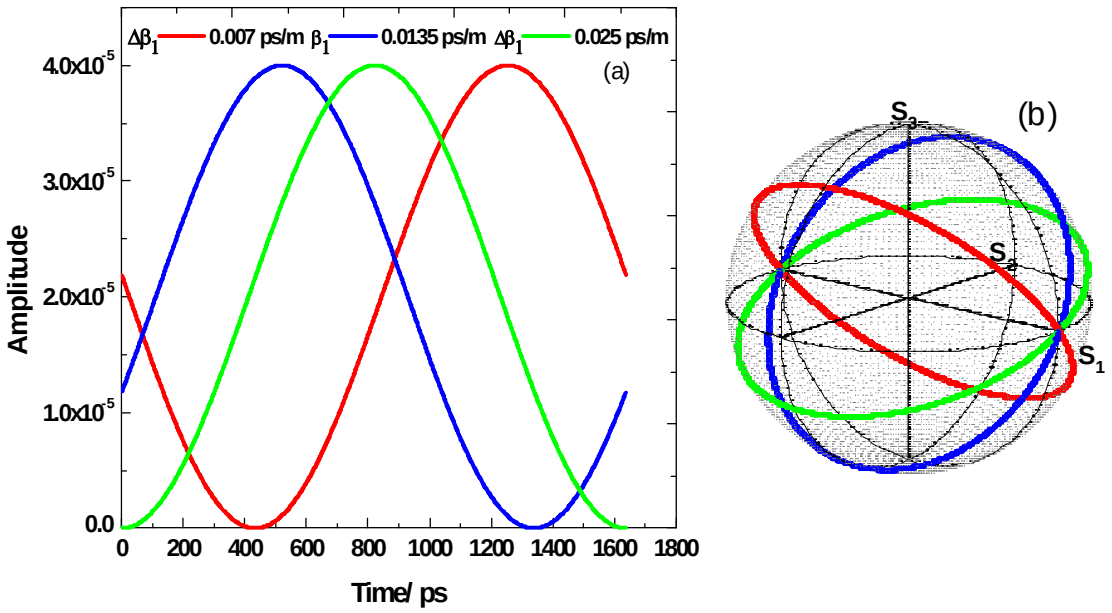

Fig. 4.1: Matlab simulation: (a) Effect of modal birefringence $\Delta\beta_1$ on the signal and (b) the corresponding Poincaré sphere representation.

At pump power of 2.8 dBm and probe power of -6 dBm, the output signal was investigated over time, at different values of modal birefringence $\Delta\beta_1$ (Fig. 4.1 (a), and the corresponding Poincaré representation given in Fig. 4.1 (b).

From Fig. 4.1 (a), the output signal varies in an oscillatory fashion and the signal broadens as the linear birefringence $\Delta\beta_1$ increases. Because of fibre birefringence, the state of polarization (SOP) of the optical signal rotates (oscillatory pattern) when propagating in the fibre. For a total phase walk-off, $\Delta\beta_1 L = 2\pi$, between the two orthogonal polarization modes, the SOP of the signal at the fibre output completes a full 2π rotation. According to Eqs. (2.6) and (2.7) in section 2.1 chapter 2, this polarization rotation can be induced by the changes of the fibre length L, the differential refractive index Δn, or the signal optical frequency ω [55]. Since the length L was a constant and birefringence is frequency independent up to first order, only the changes in modal birefringence caused the linear rotations as observed above. Also, since linear polarizations trace a circle at the equator of the Poincaré sphere (see discussions in subsection 2.1.2, chapter 2), then the overall result of birefringence is just a rotation of the signal State of Polarization (SOP) on the Poincaré sphere as shown in Fig. 4.1 (b).

4.3 The Effect of Pump Power on the Probe Signal

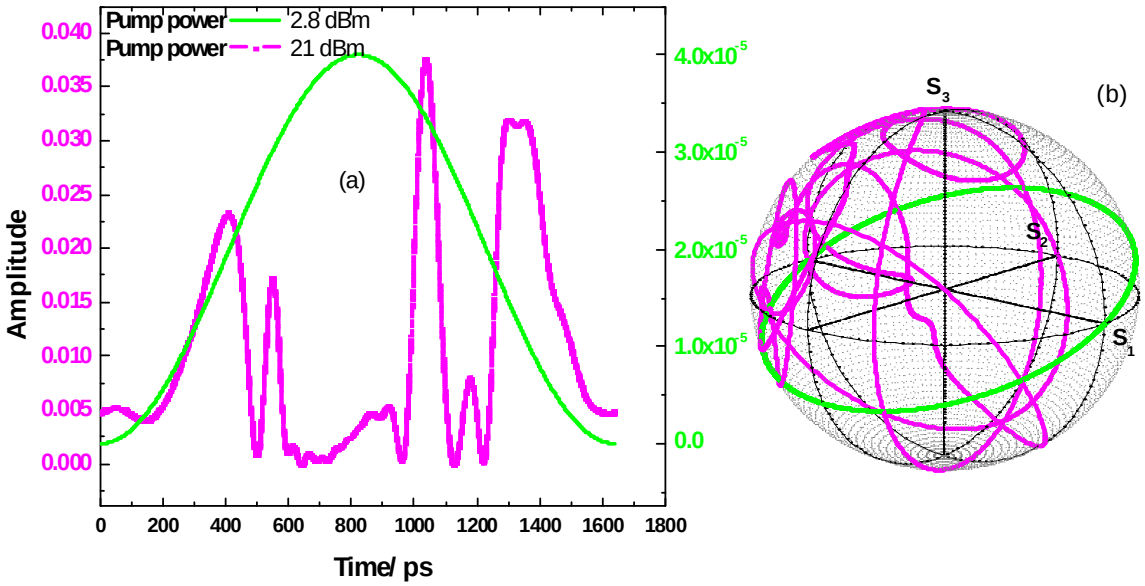

Fig. 4.2: Matlab simulation: Graphs showing (a) the effect of high pump power on the probe signal and (b) the corresponding Poincaré sphere representation.

Figure 4.2 gives results for simulations done at a constant modal birefringence, $\Delta\beta_1$ = 0.025 ps/m, and low probe power of -6 dBm. At pump power of 2.8 dBm and 21 dBm, the probe output signal was investigated over time (Fig. 4.2 (a) and the corresponding SOPs represented as shown in Fig 4.2 (b). It is observed that when the pump power is relatively low (2.8 dBm), the probe signal is sinusoidal (Fig. 4.2 (a) and traces a uniform circle on the Poincaré sphere (discussed in section 4.1), but when the pump power is increased to 21 dBm, there is more formation of peaks on the output probe signal. This is because the induced nonlinear polarization rotations (NPR) due to high pump power results into different polarization states of the probe signal and each state carries its own power. Also, looking at the Poincaré sphere, there is no periodicity and the output signal scatters in most parts of the sphere (magenta line), implying that the signal is degraded. Nonlinearity becomes significant at pump powers above 3 dBm [56].

4.4 Dependence of Probe Signal DOP on the Orientation of Pump Signal SOPs

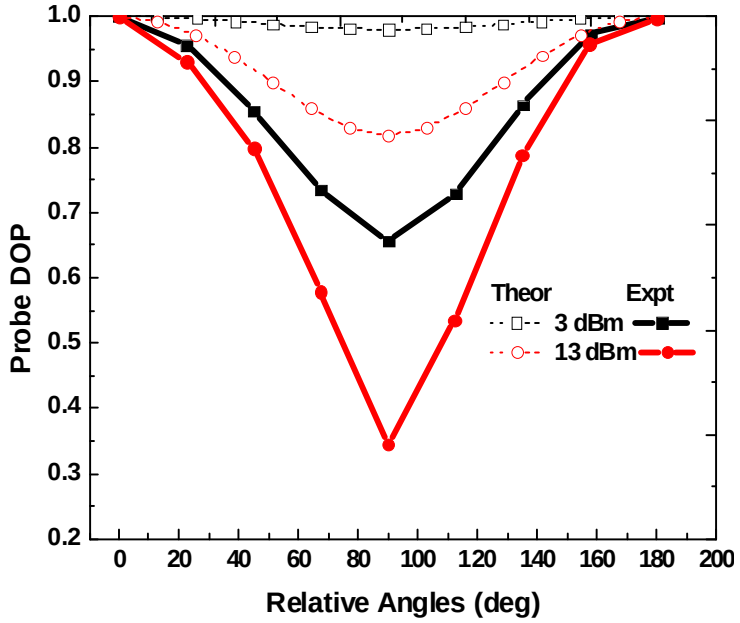

Fig. 4.3: Variation of probe DOP with relative angles for fibre length 1.7 km.

From Fig. 4.3, it is observed that the rotation of the pump signal SOPs has a high effect on the probe signal, as the relative angles between SOPs of probe and pump signal approach 90^o, but the probe signal is less affected when the relative SOPs are launched parallel (0^o) or anti parallel (180^o) in frequency domain. When the input SOPs of the probe and pump signals were launched at 90^o from each other, the depolarization of the probe signal increased with increasing pump input power; however, if the launching angle was 0^o or 180^o, increasing the pump power did not affect the probe signal. This implied that the non-linear birefringence penalty was high (low DOP) when the signal input SOPs in the two channels were perpendicular to one another. On the other hand, when the signal input SOPs were parallel or anti-parallel to each other, the nonlinear birefringence penalty was very low. This is because at 90^o the power is coupled equally into the two birefringent axes, and therefore the interaction is strong but when the

relative signal SOPs are parallel or anti-parallel to each other, there is weak interaction between the signals, resulting in a minimal nonlinear birefringence effect. The difference in experimental and theoretical results in Fig. 4.3 (previous page), was due to the power losses at the used for connecting the fibre components. The power losses can be minimized by cleaning the fibre and its components and reducing the number of splicing points and the mid couplers used for connecting fibre components.

4.5 The Effect of Linear and Nonlinear Birefringence in Different Links

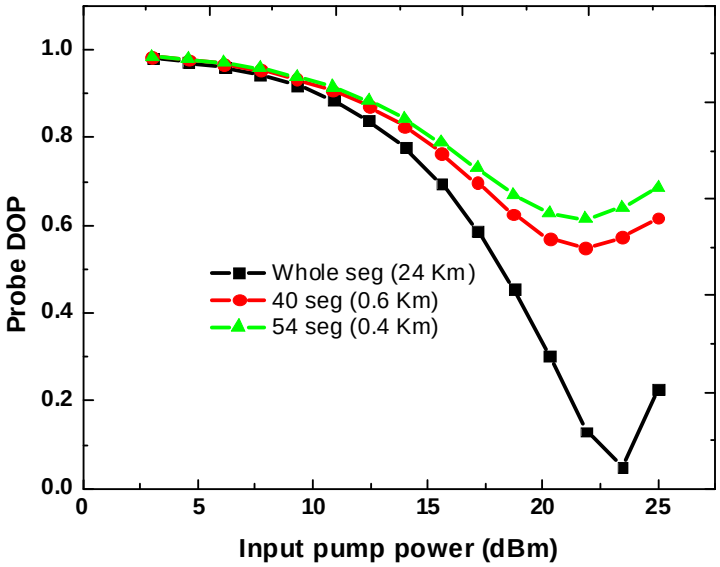

Fig. 4.4: The variation of DOP of the probe signal as a function of the input pump power for different links from Optiwave simulation.

The input power of the pump signal was varied from 3 - 25 dBm, while that of the probe was kept constant at 3 dBm. As shown in Fig. 4.4, the DOP of the probe was investigated as a function of the input pump power in the presence of non-linear birefringence alone (whole segment) and also in the presence of both non-linear and linear birefringence (40 and 54 segments). It is observed, that in a link without mode

coupling, the DOP decreases more with increasing input pump power. In other words, the nonlinear birefringence increases with the input pump power. Since the 24 km spool has low intrinsic birefringence, the relative states of polarization of the channels are preserved over a distance long enough for nonlinear polarization to occur. The nonlinear birefringence therefore, breaks the degeneracy, rotates and scatters the SOPs over large angles. Since the random birefringence in a fibre causes the output SOP vector to change, then the deviation or scattered angle measured between two output SOP vectors can be used as a measure of the birefringence effect.

In Fig. 4.5 below, the scattering angles were investigated as the input pump power increased.

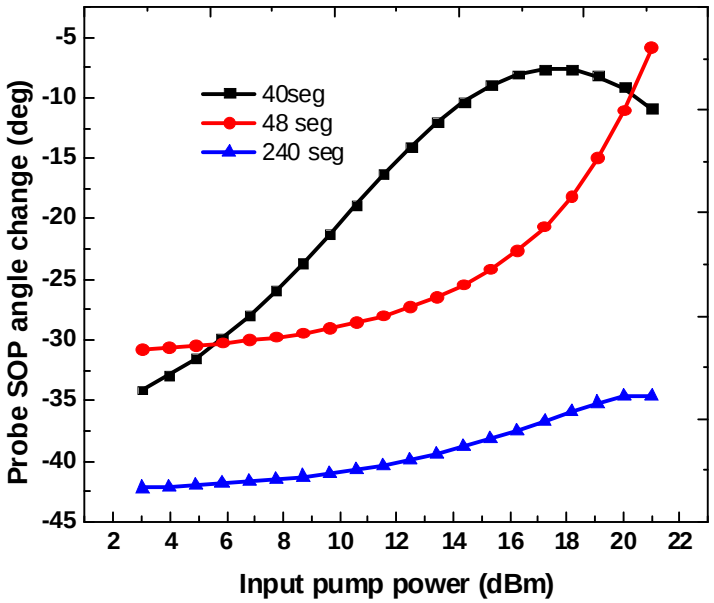

Fig. 4.5: Probe SOP angles as a function of the input pump power for different links from Optiwave simulation.

When the input pump power increases, there is an observable effect of the nonlinear birefringence on the probe signal through all the three links. Since the nonlinear birefringence rotates the polarization vector in the opposite direction to linear birefringence, it is probable that due to non-linear birefringence effects, the SOPs of the signal in one segment, are rotated such that the principal state of polarization (PSP) from the previous fast axis/slow axis is aligned to the slow/fast axis of the next segment. This reduces the resultant linear birefringence vector, and yields the low scattering angles of the SOPs, as observed in Fig. 4.5. Another explanation could be the effect of nonlinear polarization rotation (NPR) on the probe signal. The NPR usually rotates the SOPs of the signal and it is known that it reduces for a larger number of couplings/segments (small coupling length L_c) [57]. This reduction is due to the increased probability that the NPR action in one trunk is compensated for by another. Generally, the nonlinear birefringence vector may be added to or subtracted from the linear birefringence vector [58]. In summary, the interaction between the linear and nonlinear birefringence in the fibre sometimes reduces the effect of nonlinear birefringence on the signal.

4.6 Dependence of Probe DOP, SOP Vector and Angles on Channel Spacing

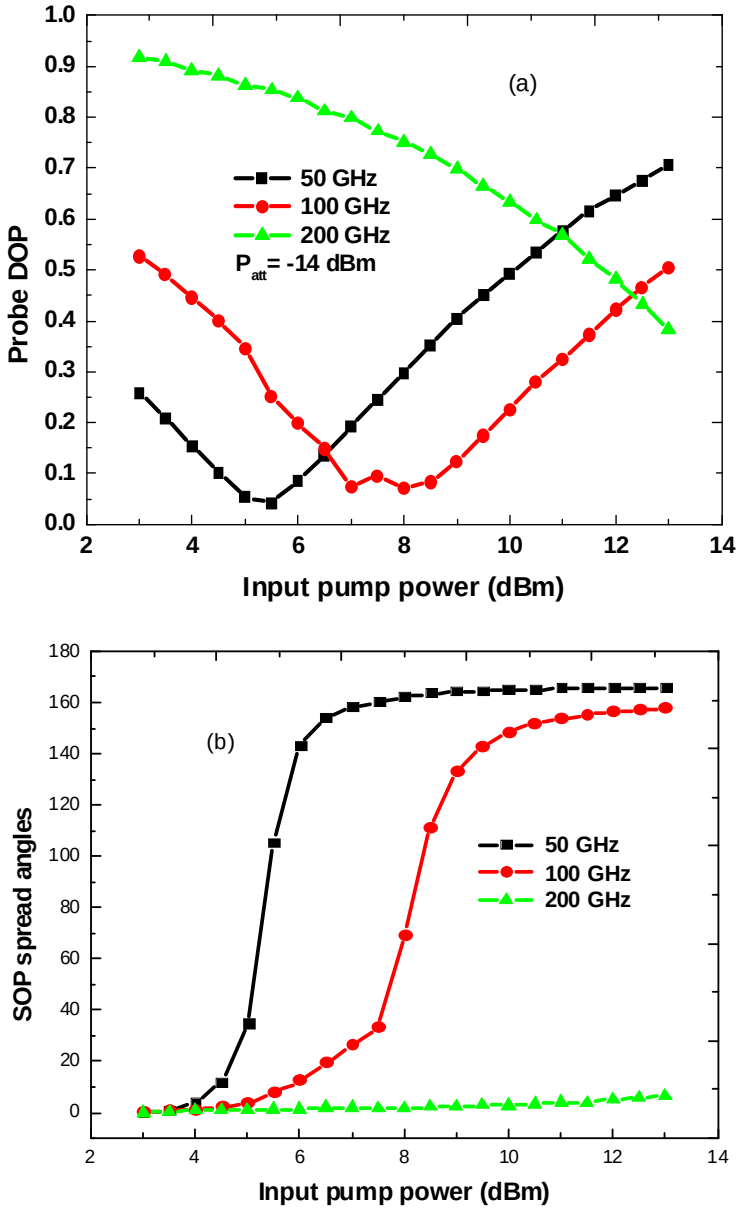

Fig. 4.6: Experimental results for (a) variation of probe DOP with input pump power (b) variation of relative SOP angles as a function of input power.

Figure 4.6 (a) shows the measured DOP of the probe signal as a function of input pump power, when the SOP of the pump was aligned at 90^{o} with respect to the probe signal. The probe input power (P_{att}) into the coupler was -14 dBm while the pump power was

in the range of 3-13 dBm. The probe signal DOP reduces drastically with increasing input power, for 50 GHz and 100 GHz channel spacing then it starts to improve after a particular value of pump power; while for 200 GHz it decreases monotonically. Nonlinear birefringence vector tends to rotate in such a way that it adds to the linear vector and cancels its existence, hence giving rise to the DOP improvement as shown in Fig. 4.6 (a) (black and red). As the channel spacing increases, the interaction between the probe and the pump signal is reduced, thus the DOP improvement for 100 GHz come later, after that of 50 GHz channel spacing. When two vectors are equal and parallel, there is a maximum polarization scattering, as indicated by the scattering angles in Fig. 4.6 (b). The SOPs for 50 GHz rotate faster due to smaller channel spacing hence, large scattering angles while for 200 GHz SOPs rotate much slower, leading to very small scattering angles, as seen in Fig. 4.6 (b). Further analysis was done on the experimental results obtained for figure 4.6 above and discussed as follows.

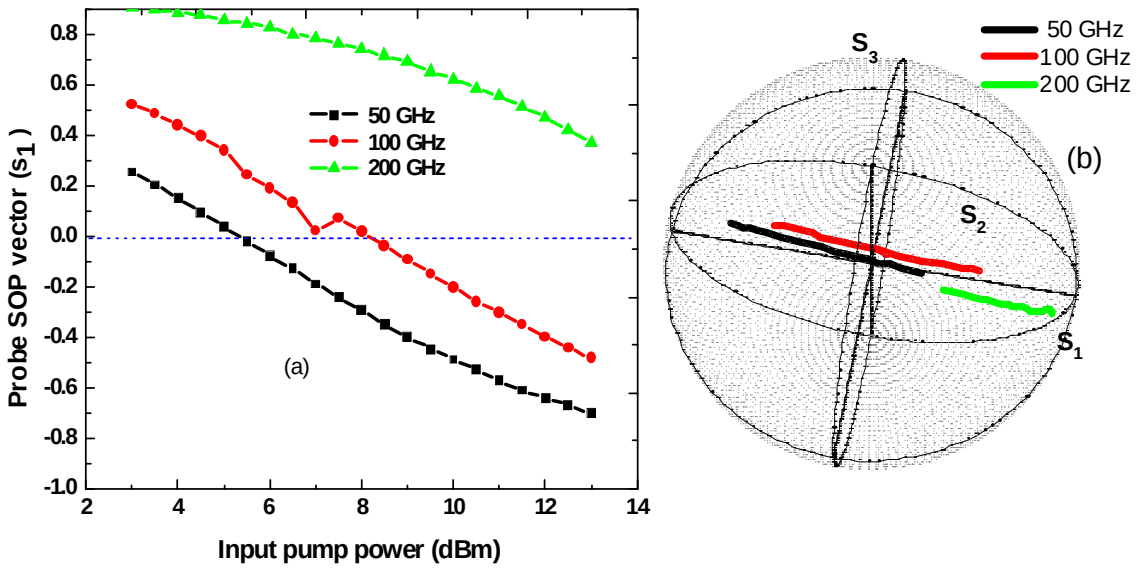

Fig. 4.7: Experimental results for (a) Probe SOP vectors against input pump power and (b) is the Poincaré sphere representation of the three SOP vectors (s_1, s_2, s_3).

Figure 4.7 (a) shows how the SOP vector (S_1) varies with input pump power. Since the graphs are linear, it implies that the vector is linear too. The influence of pump power is the rotation of the vector and the change in its direction (crossing of the blue line). As the channel spacing increases, the corresponding values of the pump power, at the turning point, also increase as seen in Fig. 4.7 (a). This is due to the interaction between the probe and the pump signals that reduces as the spacing increases, such that it will require larger pump power to cause the change in the vectors direction, as in the case of 200 GHz channel spacing. The states of polarization given by the vectors s_1, s_2 and s_3 for different channel spacing are clearly depicted in Fig. 4.7 (b) and is dominated by s_1 since it's along its axis. Thus, the variation of DOP in Fig. 4.6 (a) and angles in Fig. 4.6 (b) is due to the movement of the vector s_1. It can also, be observed that for 50 GHz channel spacing where there is high interaction, the vector s_1 has already crossed into the other half of the sphere, closer to the pump axis, followed by s_1 for 100 GHz; while s_1 for 200 GHz trails behind them and has not even crossed. It's like the pump rotates and pulls the vector s_1 towards its axis and once it has crossed the s_2-s_3 axis, it acquires the same sign as the nonlinear vector, which leads to improved DOP.

4.7 Effect of Attenuation on the Probe Signal.

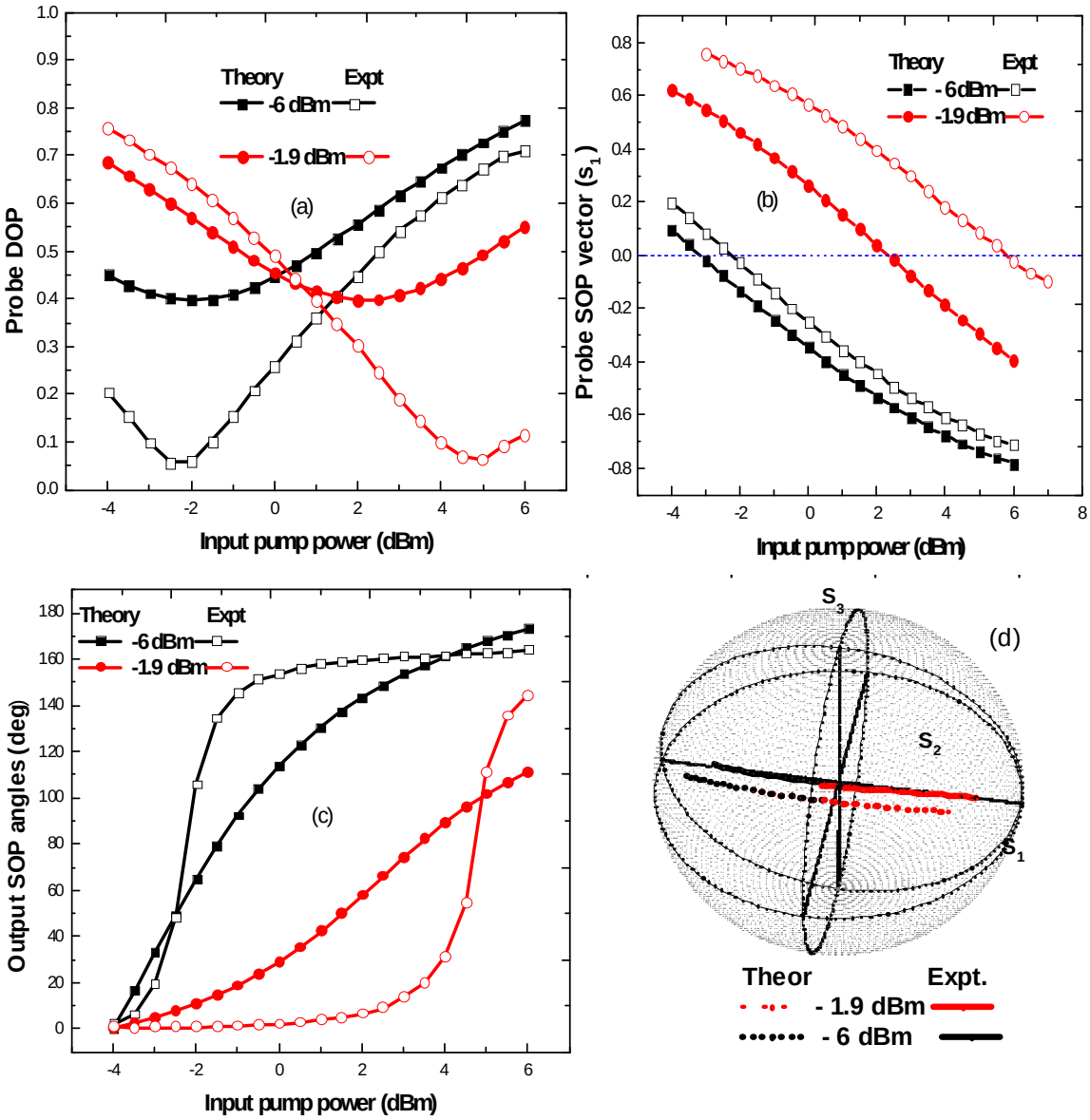

Fig. 4.8: (a) Variation of probe DOP with input pump power (b) variation of SOP with input pump power (c) variation of relative SOP angles as a function of input power and (d) is the Poincaré sphere representation of the three SOP vectors (s_1, s_2, s_3).

In figure 4.8, a channel spacing of 50 GHz (0.4) was used and pump power was varied from -4 dBm to 6 dBm, while the probe power was -6 dBm and -1.9 dBm. It is observed from Fig. 4.8 (a) that when the input probe power is -6 dBm the turning point/effect is

realized earlier than for the case of -1.9 dBm. As the relative magnitude power between the probe and the pump increases, more pump power fluctuates into the probe axis and alters the orientation of the probe SOPs much faster. Thus, when the input probe power is -6 dBm, the SOP vector changes its direction (crossing of the blue line) much earlier than in the case of -1.9 dBm, as seen in Fig. 4.8 (b). The point at which the vector changes its direction becomes the turning point and it implies that at that point, the linear and nonlinear birefringence cancels out. Also, from Fig. 4.8 (c) the rate of angle spread is higher when the probe input power is -6 dBm than when it is -1.9 dBm. This is because the SOP vector rotation is much faster when the relative power between the pump and the probe is high. This is also, evident on the Poincaré sphere Fig. 4.8 (d), where the vector s_1 for -6 dBm precedes that of -1.9 dBm and crosses the s_2-s_3 axis much earlier. The difference in experimental and simulated results can be due to attenuation of the probe signal at the connectors and spliced points, while for simulations, an ideal condition was assumed.

4.8 Characteristics of a Designed Stress Sensor

In this experiment, two different fibres were used (PMF and LEAF) as sensing elements, where the channel spacing between the pump and the probe was 50 GHz (0.4 nm) and the relative input polarization angle between the pump and the probe SOPs was 90^0. A channel spacing of 0.4 nm was used because from the results in section 4.6, it gives the highest interaction between the pump and the probe signals. The sensor was optimized at different pump-probe power ratios PR, and at each value of PR, the pump channel at R-section in Fig 3.1, was subjected to varying weights within the range of

2.5-32.5 kg. The output probe DOP was then measured (Fig. 4.9 (a) and (c)). The sensing length (10.5 cm) was sandwiched between two thin transparent plastic sheets, to cover the sensor for protection against stress concentration.

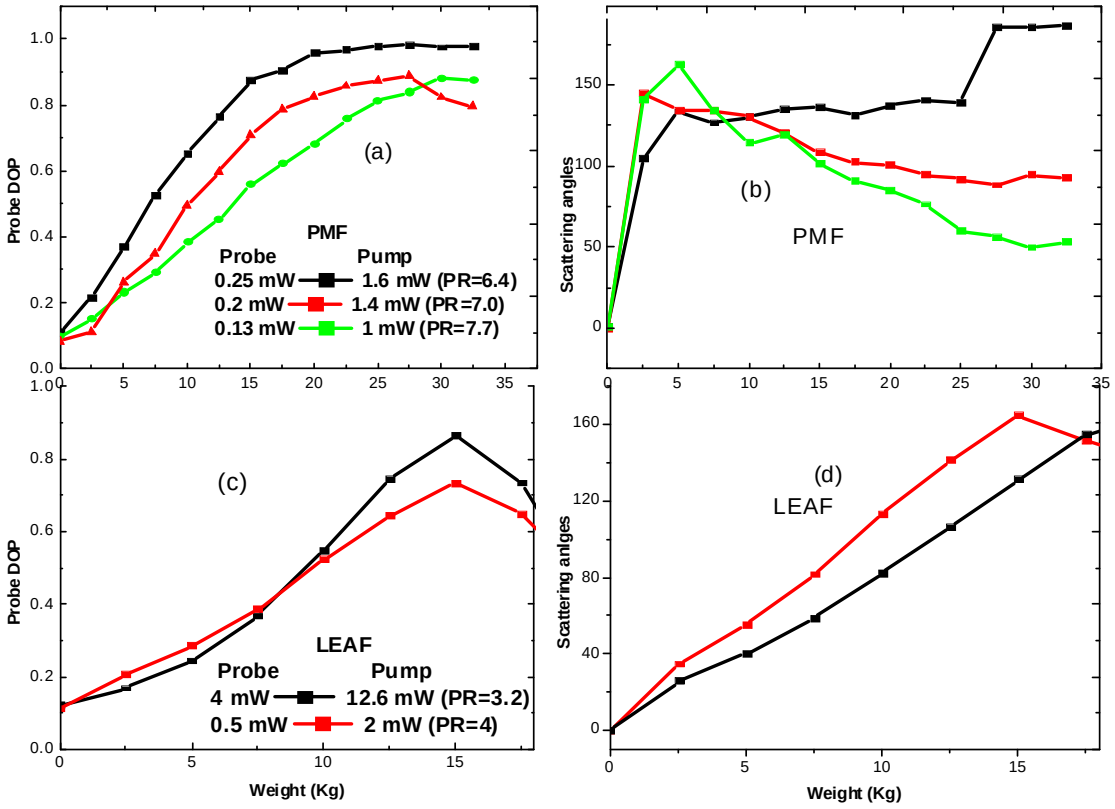

Fig. 4.9: Experimental results for the stress sensor using (a) polarization maintaining fibre (PMF) and (c) LEAF fibre. Corresponding scattering angles are given by (b) and (d).

It is observed that the DOP of the probe increases approximately linearly with increase in weight, up to 27.5 kg for PMF and 15 kg for LEAF. The weight applied at the sensing length along the pump channel introduces an additional birefringence (Eq. (2.25) as discussed under subsection 2.5.4 of chapter 2). According to equation (2.8) in subsection 2.1.4, chapter 2, the induced birefringence simply rotates the SOPs of the pump, which in turn, linearly orientate those of the probe, hence, improved DOP.

Mathematically, it can be argued that increase in birefringence reduces the walk-off length L_w (check subsection 2.5.4), which in turn reduces the argument of the Bessel function in Eq. (2.30) subsection 2.5.4, thus, improved DOP in Eq. (2.31) (same subsection), since the term $\langle \cos\Delta\psi(t) \rangle$ increases. The sensor operates effectively up to a maximum critical weight beyond which the DOP tends to remain unchanged (black line for PMF), or drops (LEAF) with increasing weights. This is because the polarization rotations of the pump has reached maximum, due to elasto-optic limit nature of the fibre.

As the pump-probe power ratio PR reduces, the sensitivity of the sensor increases. For PMF fibre (PR = 6.4) has higher sensitivity per unit weight of 0.051 kg^{-1}, followed by 0.045 kg^{-1} (PR = 7.0) and lastly, 0.034 kg^{-1}(PR = 7.7); while LEAF fibre (PR = 3.2) has sensitivity of 0.049 kg^{-1}, higher than that of 0.041 kg^{-1}(PR = 4). Reduction in PR leads to reduced θ_s, according to the expression given in the paragraph above Eq. (2.28), found in subsection 2.5.4. When θ_s is small, it reduces the value of the sine in Eq. (2.31) hence, improved sensitivity. It also, implies that the scattering on the probe signal has been minimized as depicted by Fig. 4.9 (b) and (d). For example, (PMF) black line which has less PR is less scattered than green. Polarization maintaining fibre (PMF) covers a wider range of weights, than large effective area fibre (LEAF). In LEAF, A_{eff} is increased intentionally, to reduce the impact of fibre nonlinearity (check Eq. (2.12) in section 2.2, chapter 2). In other words, the LEAF fibre is a highly birefringent fibre thus; it reaches its elasto-optic limit much earlier.

4.9 Strain Sensor

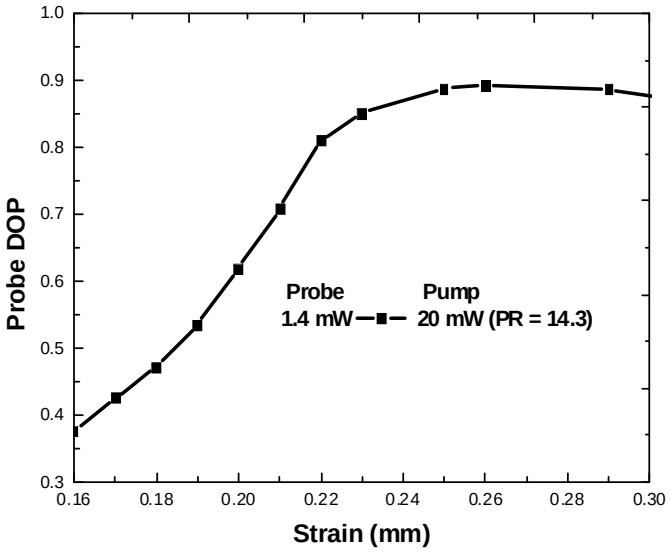

Fig. 4.10: Experimental results for a strain sensor using a single mode fibre (SMF) as the sensing fibre.

A section of polarimetric optical fibre strain sensor was embedded in two plastic sheets, similar to those used in section 4.8. A micrometer screw gauge was used, to induce strain on the plastic sheets, by means of tightening. The DOP of the probe was then measured as strain (function of displacement/extension) was increased. From Fig. 4.10, it is observed that the DOP of the probe varies as the strain increases and saturates when strain is above 0.25 mm. This could be attributed to the fact that the compressive strain experienced by the plastic sheets is transferred to the fibre, and a strain-induced rotation of the birefringence axes occurs as a result of the photo-elastic effect [48]. The polarization state of the output probe light thus, changes as the birefringence axes of the pump rotate but when the SOPs of the pump and probe are anti-parallel, there is weak interaction between the pump and the probe (as discussed in section 4.4) hence

constant DOP after strain of 0.25 mm. The sensitivity of the sensor was determined to be 0.0103 μm^{-1} by getting the gradient of the graph.

4.10 Temperature Sensor

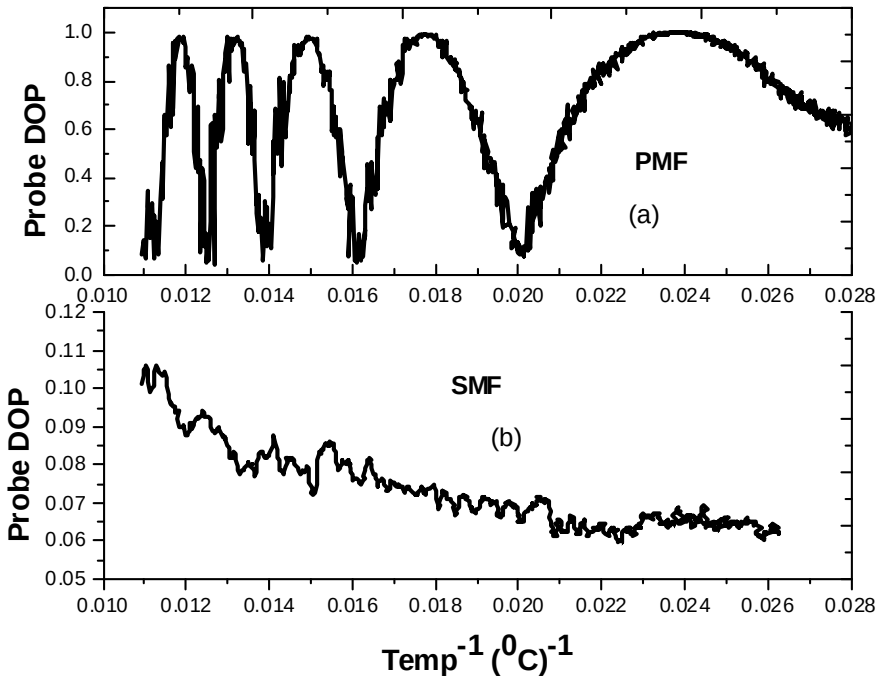

Fig. 4.11: Experimental results for temperature sensor using (a) PMF (b) SMF.

In this particular experiment, the sensing length was immersed in a jar containing water that was heated to approximately 100 ^{0}C and allowed to cool. The cooling was not forced but exposed to the normal ambient conditions. A thermocouple was used to measure temperature, as the DOP of the probe was monitored, with decrease in temperature. Figure 4.11 (a) shows that the DOP of probe for a PMF varies as a sinusoidal function of temperature. At high temperatures, the rate or frequency at which the DOP varies is faster than at lower temperatures. Temperature-induced rotations

reduce as the water cools, resulting in slower DOP variations as observed in Fig. 4.11 (a) and vice versa. Similarly, for single mode fibre, as the temperature reduces, temperature-induced rotations reduce, hence, DOP also reduces as observed in Fig. 4.11 (b). The sensitivity for SMF was very small (0.0009 $^{0}C^{-1}$), implying that the sensor was less sensitive to temperature variations, thus, PMF fibre would be the best choice as a sensing element since it has a higher sensitivity of 0.181 $^{0}C^{-1}$ over a range of 34-90.9 ^{0}C.

CHAPTER 5

CONCLUSIONS AND RECOMMENDATIONS

5.1 Conclusions

The important findings of the study are summarized in this chapter. The rotations of SOPs due to linear birefringence alter the shape of the signal. The effect of nonlinear birefringence-induced polarization rotation in a fibre depends on the orientation of the relative input polarization vectors of co-propagated channels and the power carried by each polarization vector. In low intrinsic birefringence link, the nonlinear induced-birefringence effects scatter the SOPs thereby depolarizing the signal. Therefore the linear and nonlinear birefringence constitute the major limiting factors of modern systems employing fibre optic elements.

The interaction between the linear and nonlinear induced birefringence in a fibre with consideration of mode coupling was investigated. For links with high polarization mode coupling, the nonlinear birefringence sometimes couples with the linear birefringence vector such that it reduces the penalty and improves the signal DOP. A sound knowledge of the interaction between linear and nonlinear birefringence led to the pump-probe scheme used in the design of fibre optic sensor. A sensor was successfully designed and the investigation show that the degree of polarization (DOP) of the probe increases linearly with the applied physical measurand (stress and strain). Further investigations show that for temperature sensing with polarization maintaining fibre (PMF) used as a sensing fibre, the rate or frequency at which the DOP varies is faster at high temperatures than at lower temperatures. The design of a stress sensor gave the

best sensitivity of 0.051 kg^{-1} over a range of 0-27.5 kg with PMF as the sensing fibre while that of strain sensor gave a sensitivity of 0.0103 μm^{-1} over a range of 0.16 -0.26 mm with single mode fibre as the sensing element. Lastly, the design of a temperature sensor gave the best sensitivity of 0.181 $^0C^{-1}$ with PMF fibre over a range of 34-90.9 ^0C. The designed sensors offer unique possibility in high accuracy and sensitivity since they take into account the three operating principles of fibre optic sensor (FOS) (intensity, phase and polarization).

From the discussions in chapter 4, a sensor can be designed according to its sensor requirements by selecting an appropriate type of fibre and by varying the relative pump-probe powers for sensor optimization. The simplicity of the design and low power requirements which results in the low cost of the fabrication is the point which makes it suitable for actual field application. The designed sensor also has a reproducible high performance, a very important factor in the operation of any sensor system.

5.2 Recommendations for further studies

In this study, polarization dependent loss (PDL) for linear and nonlinear interaction in the fibre was assumed to be negligible. Therefore it is recommended that an investigation be carried out to account for the effects of PDL in the interaction of linear and nonlinear birefringence on the signal. The wavelength division multiplexing (WDM) laser source used in the experimental work could not provide power above 13 dBm which limited investigations of nonlinear effects for pump powers above 13 dBm.

For further research it is recommended that the investigation be carried out in this respect.

The pump-probe scheme uses only two channels; there is an open door for investigations for many inter-channel interactions but using the same principles as the ones employed in this study for possibility of other sensor designs. Also, from the laser source the minimum channel spacing that could be obtained was 50 GHz (0.4 nm); further investigations should be done using channel spacing less than 0.4 nm as it will give more interaction between the channels. In order to increase the sensitivity of the temperature sensor, it is recommended that a thermosensitive cladding of the fibre be used. Last but not least, for temperature sensor, investigations were done up to a minimum temperature of 34^0, it is recommended that investigations be done below this temperature. Generally, fibre optic sensor technology offer unique possibilities in a measurement context and where this will lead depends particularly on the initiatives of the research community.

REFERENCES

[1] P. Cochrane, *Optical Network Technology*. Chapman Hall, 1st edition, (1995).

[2] B. Mukherjee, *Optical Communication Networks*. McGraw-Hill, 1st edition, (1997).

[3] T. Karause and R. Castelli, "Market trends and evolution for optical transmission systems,'' Alcatel Telecommunication Review, pp. 165-175, 3rd Quarter (1998).

[4] G.P. Agrawal, *Nonlinear Fibre Optics*. San Diego Califonia: Academic press 2nd edition, (1995).

[5] P.D. Maker, R.W. Terhune and C.M. Savage, ''Intensity-dependent changes in the refractive index of liquids,'' Physics Review Letter, 12 507–9, (1964).

[6] J. Toulouse, ''Optical Nonlinearities in Fibres: Review, Recent Examples, and Systems Applications,'' Journal of Light-wave. Technology, Vol. 23, no. 11, pp 3625, Nov. (2005).

[7] D. Derickson, *Fibre Optic: Test and Measurement.* chapter 6, Prentice Hall, (1998).

[8] M. Born and E. Wolf, *Principles of Optics.* 7th ed., chapter 10, Cambridge University press, (1999).

[9] S.C. Rashleigh and R. Ulrich, "Polarization mode dispersion in singlemode fibres," Optics Letter, Vol. 3(2), pp. 60-62, (1978).

[10] M. Karlsson, "Polarization mode dispersion–induced pulse broadening in optical fibres," Optics Letter, Vol. 23(9), pp. 688-690, (1998).

[11] C.D. Poole and C.R. Giles, "Polarization-dependent pulse compression and broadening due to polarization dispersion in dispersion-shifted fibre," Optics Letter, Vol. 13(2), pp. 155-157, (1988).

[12] P.M. Krummrich, J. Rösch and J. Wuttke, "Polarization Oscillations in Aerial Fibre Caused by Wind and Power-Line Current," IEEE Photon Technology Letter, Vol. 15(6), pp. 882-884, (2003).

[13] D.S. Waddy, L. Chen and X. Bao, ''Invited paper on Polarization effects in aerial fibres," Optical Fibre Technology, Vol. 11, pp.1–19, (2005).

[14] C.R. Menyuk and A. Galtarossa, *Polarization Mode Dispersion.* 1st edition, chapter 1, Springer, (2005).

[15] J.D. Kraus, *Electromagnetics*. 3rd Edition, McGraw-Hill, New York, NY, USA, (1984).

[16] C.R. Menyuk and R. Galtarossa, *Polarization Mode Dispersion.* 1st edition, chapter 2, Springer, (2005).

[17] F. Curti, B. Diano, Q. Mao and F. Matera, "Concatenation of polarization dispersion in single-mode fibres," Electronics Letter, Vol. 25(4), pp. 290-292, (1989).

[18] H. Paul, "Polarization mode dispersion measurement by the Jones matrix Eigenanalysis and wavelength scanning methods," Hewlett Packard Light-wave operations Technical report, Santa Rosa, CA, USA, January (1997).

[19] C.D. Poole and R.E. Wagner, "Phenomenological approach to polarization mode dispersion in long single mode fibres," Electronics Letters, Vol. 22, No. 19, pp. 1029-1030, Sep 11, (1986).

[20] Y. Mauricio, ''Pulse Narrowing in Optical Fibres with Polarization Mode Dispersion,'' Msc Thesis, University of New Brunswick, pp. 11, May (2000).

[21] J.P. Gordon and H. Kogelnik, "PMD fundamentals: Polarization mode dispersion in optical fibres," Proceedings of National Academy of Sciences, Vol. 97(9), pp. 4541- 4550 [Online]. Available: http://www.pnas.org., (2000).

[22] G.E. Keiser, *Optical Fibre Communications.* 3rd edition, McGraw Hill, New York, Chapter 8, (1999).

[23] M. Lax, J.H. Batteh, and G.P. Agrawal, ''Channeling of Intense Electromagnetic Beams,'' Journal of Applied Physics, vol. 52, no. 1, pp. 109-125, (1981).

[24] G.P. Agrawal, "Self-phase modulation and spectral broadening of optical pulses in semiconductor laser amplifiers," IEEE Quantum Electron, Vol. 25(11), pp. 2297-2306, (1989).

[25] R.H. Stolen and C. Lin, "Self phase modulation in silica optical fibres," Physics Review, vol. 17, no. 4, p. 1448, (1978).

[26] J.M. Dudley, A.C. Peacock, and G. Millot, "The cancellation of nonlinear and dispersive phase components on the fundamental optical fibre soliton: A pedagogical note," Optical Communication, vol. 193, no. 1–6, pp. 253–259, Jun. 15, (2001).

[27] M.N. Islam, L.F. Mollenauer, R.H. Stolen, J.R. Simpson, and H.T. Shang, "Cross-phase modulation in optical fibres," Optics Letter, vol. 12, no. 8, p. 625, Aug. (1987).

[28] V.E. Perlin and H.G. Winful, "Nonlinear pulse switching using crossphase modulation and fibre Bragg gratings," IEEE Photon Technology Letter, vol. 13, no. 9, pp. 960–962, Sep. (2001).

[29] R. Hui, K.R. Demarest, and C.T. Allen, "Cross-phase modulation in multispan WDM optical fibre systems," Journal of Light-wave Technology, vol. 17, no. 6, pp. 1018–1026, Jun. (1999).

[30] B.C. Collings and L. Boivin, "Nonlinear polarization evolution induced by cross-phase modulation and its impact on transmission systems," IEEE Photon Technology Letter, vol. 12, no. 11, pp. 1582–1584, Nov. (2000).

[31] G.P. Agrawal, *Nonlinear Fibre Optics*. 3rd edition, San Diego, CA: Academic press 206, (2001).

[32] Q. Lin and G.P. Agrawal, "Vector theory of cross-phase modulation: Role of nonlinear polarization rotation," IEEE Journal Quantum Electron, vol. 40, no. 7, pp. 958–964, Jul. (2004).

[33] G.E. Keiser, *Optical Fibre Communications.* 3rd edition, McGraw Hill, New York, Chapter 8, (1999).

[34] K. Inoue and H. Toba, "Error rate degradation due to fibre four-wave mixing in a 4-channel FSK direct detection transmission,'' IEEE Photon Technology Letter, Vol. 3(1), pp. 77-79, (1991).

[35] B.C. Collings and L. Boivin, "Nonlinear polarization evolution induced by cross-phase modulation and its impact on transmission systems," IEEE Photon Technology Letter, Vol. 12(11), pp. 1582-1584, (2000).

[36] A. Bononi, A. Vannucci, A. Orlandini, E. Corbel, S. Lanne and S. Bigo, "Degree of polarization degradation due to cross-phase modulation and its impact on polarization-mode dispersion compensator," Journal of Light-wave Technology, Vol. 21(9), pp. 1903-1913, (2003).

[37] P.K.A. Wai and C.R. Menyuk, "Polarization mode dispersion, decorrelation and diffusion in optical fibres with randomly varying birefringence," Journal of Light-wave Technology, Vol. 14(2), pp. 148-157, (1996).

[38] P.K.A. Wai, W.L. Kath, C.R. Menyuk and J.W. Zhang, "Nonlinear polarization-mode dispersion in optical fibres with randomly varying birefringence," Optical Society of America, Vol. 14(11), pp. 2967-2979, (1997).

[39] V. Kermène, M.T. Flores-Arias, J. Ares, A. Desfarges-Berthelemot and A. Barthélémy, “Nonlinear polarization evolution: a numerical study of the coupling between main linear normal modes,” Optical Communications, Vol. 247, pp. 195-203, (2005).

[40] S.N. Thiam and F.A. Rahman, “A model to characterize the effect of cross phase modulation on polarization in an optical fibre transmission system,” International Journal of Light and Electron, Vol. 118(7), pp. 507-514, (2007).

[41] D.A. Krohn, *Fibre Optic Sensors-Fundamental and Applications*. Instrument Society of America, (1988).

[42] D. Donlagic, ‘‘Fibre optic sensors: An introduction and overview,’’ Smetanova ulica 17, Maribor, (2000).

[43] B. Gholamzadeh and H. Nabovati, ‘‘Fibre Optic Sensors,’’ World Academy of Science, Engineering and Technology 42, (2008).

[44] H. Golnabi, ‘‘Design of an optical fibre sensor for linear thermal expansion measurement,’’ Optics and Laser Technology 34, pp 389-394, (2002).

[45] F. Yu and S. Yin, *Fiber optic sensors*. Marcel-Dekker, (2002).

[46] A.W. Damanski, T.R. Wolinski and W.J. Bock, ‘‘Polarimetric fibre optic sensors: state –of-the-art and future,’’ Proc SPIE, (1995).

[47] H.M. Xie, P. Dabkiewicz, R. Ulrich, and K. Okamoto, “Side-hole fibre for fibre optic pressure sensing,” Optics Letter, vol. 11, no. 5, pp. 333–335, (1986).

[48] G. Liu and S. Chuang, “Polarimetric optical fibre weight sensor,” Sensors and Actuators, vol. 69, pp. 143–147, (1998).

[49] Z. Pan, Q. Yu, A.E. Willner, and Y. Arieli, “Fast XPM-induced polarization-state fluctuations in WDM systems and their mitigation,” in Proc. OFC 2002, Anaheim, CA, Paper ThA7, pp. 379–381. (2002).

[50] A. Vannucci, A. Bononi, A. Orlandini, E. Corbel, J.P. Thiéry, S. Lanne, and S. Bigo, “A simple formula for the degree of polarization degraded by XPM and its experimental validation,” in Proc. OFC 2003, Atlanta, GA, Paper ThJ1, Feb. (2003).

[51] J.H. Lee, "Analysis and Characterization of Fibre Nonlinearities with Deterministic and Stochastic Signal Sources." D.Phil Thesis. University of Virginia, Blacksburg, pp. 18, (2000).

[52] R.J. Essiambre, and G.P. Agrawal, ‘‘Timing Jitter of Ultrashort Solitons in High Speed Communication Systems II. Control of Jitter by Periodic Optical Phase Conjugation,’’ Journal of Optical Society, B 14, pp. 323, (1997).

[53] C.G. Goedde, W.L. Kath and P. Kumar, ‘‘Periodic Amplification and Conjugation of Optical Solitons,’’ Optics Letter, 20, Issue 12, pp. 1365-1367, (1995).

[54] M.E. Marhic, A.A. Rieznik, G. Kalogerakis, C. Braimiotis, H.L. Fragnito and L.G. Kazovsky, ‘‘Accurate Numerical Simulation of Short Fibre Optical Parametric Amplifiers,’’ Optics Exp, vol 16, No. 16, pp. 3610-3622, (2008).

[55] R. Hui and M. O’Sullivan, *Fibre Optic Measurement Technique.* Elsevier: USA, pp. 409-410, (2009).

[56] E.K. Rotich, ‘‘Modeling of a Fibre Optical Parametric Amplifier Based on Four Wave Mixing,’’ Msc Thesis, Moi University, Eldoret, pp 47-48, (2012).

[57] C. Vinegoni, M. Wegmuller, and N. Gisin, ‘‘Determination of the polarization coupling length in telecom fibres exploiting the nonlinear polarization rotation,’’ Group of Applied Physics - Gap Optique, University of Geneva, (2001).

[58] C. Vinegoni, M. Wegmemuller, B. Huttner and N. Gisin, “Measurement of nonlinear polarization rotation in a highly birefringent optical fibre using a Faraday mirror,” Journal of Optical Society: Pure Applied Optics, Vol. 2, pp. 314-318, (2000).

APPENDICES

Appendix A

Publications, Conference Presentations and Research Visits

Publications and Conference Presentations

1. S. Kuja, E.K. Rotich Kipnoo, D.K. Boiyo, D. Waswa and G. Amolo, ‘‘Interaction between the Linear and Nonlinear Polarization in Optical Fibre,’’ *8th Moi University International Conference*, 4th-8th Sep. 2012 – in press.

2. D. Kiboi Boiyo, S. Kuja, E. Rotich Kipnoo, G. Amolo and D. Waswa, ‘‘Modelling of an Optical Fibre Raman Amplifier,’’ *8th Moi University International Conference*, 4th - 8th Sep. 2012 – in press.

3. D. Kiboi Boiyo, S. Kuja, E. Rotich Kipnoo, G. Amolo and D. Waswa, ‘‘Characterization of an Optical Fibre Raman Amplifier,’’ 7th *Egerton University International Conference and Expo*-26-28th Sep. 2012 - Accepted.

Research Visit

- Optical Fibre Technologies Research and Discussions, Nelson Mandela Metropolitan University, Port Elizabeth, South Africa, 23rd March 2012-14th June 2012.

Appendix B

Experimental set up for fibre sensors

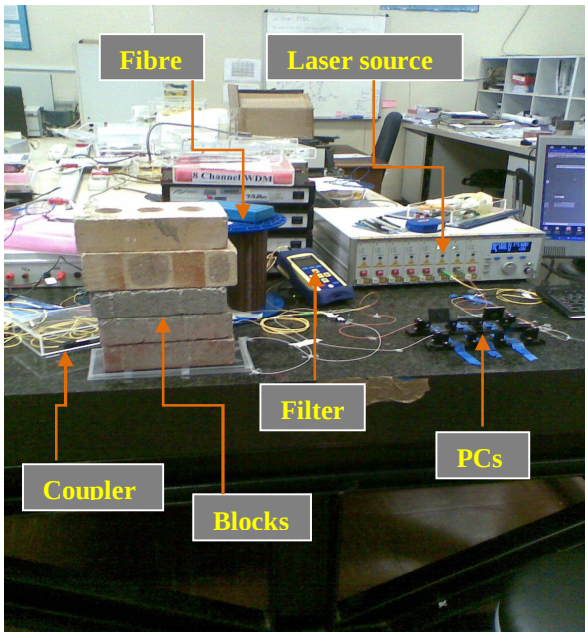

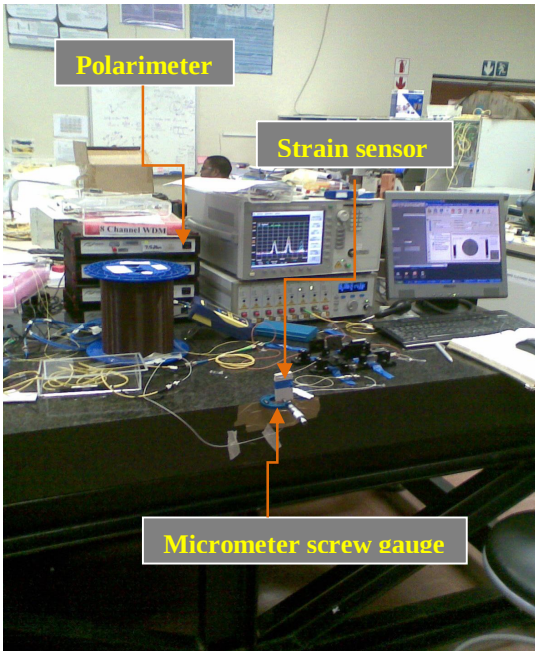

Appendix C

Experimental results showing how the probe SOP vectors (s_1, s_2, s_3) vary with input pump power.

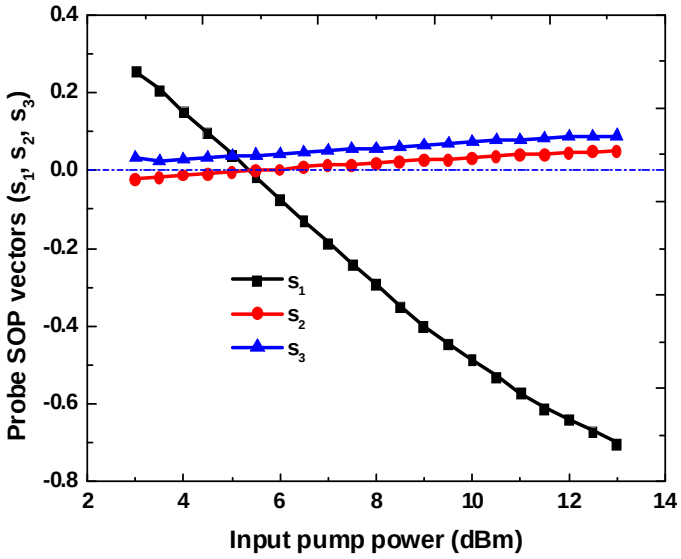

Fig. C.1: Probe SOP vectors (s_1, s_2, s_3) against input pump power for 50 GHz channel spacing.

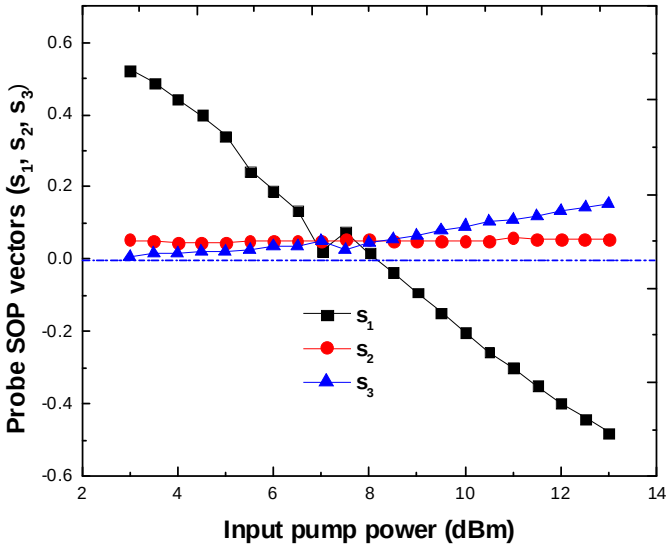

Fig. C.2: Probe SOP vectors (s_1, s_2, s_3) against input pump power for 100 GHz channel spacing.

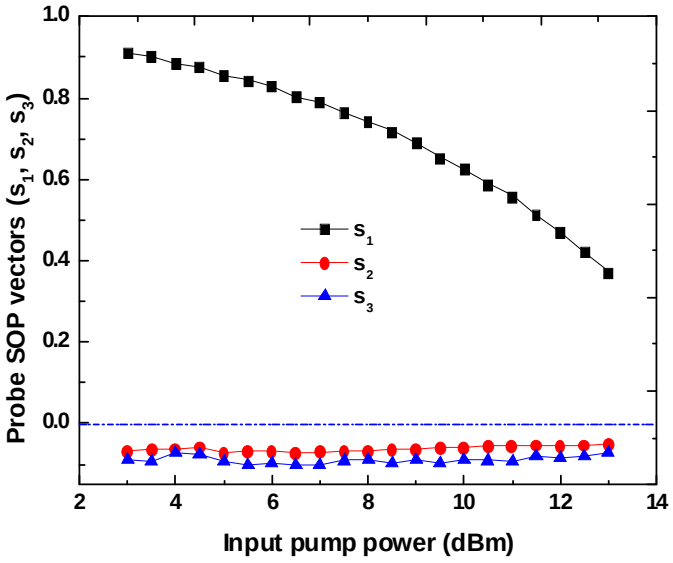

Fig. C.3: Probe SOP vectors (s_1, s_2, s_3) against input pump power for 200 GHz channel spacing.